Mathematical Medicine and Biology (2007) **24**, 347–377
doi:10.1093/imammb/dqm004
Advance Access publication on October 17, 2007

Single-equation models for the tear film in a blink cycle: realistic lid motion

A. HERYUDONO, R. J. BRAUN†, T. A. DRISCOLL, K. L. MAKI AND L. P. COOK
Department of Mathematical Sciences, University of Delaware, Newark, DE 19711, USA

AND

P. E. KING-SMITH
College of Optometry, The Ohio State University, Columbus, OH, USA

[Received on 16 March 2007; revised on 18 July 2007; accepted on 19 July 2007]

We consider model problems for the tear film over multiple blink cycles that utilize a single equation for the tear film; the single non-linear partial differential equation that governs the film thickness arises from lubrication theory. The two models that we consider arise from considering the absence of naturally occurring surfactant and the case when the surfactant is strongly affecting the surface tension. The film is considered on a time-varying domain length with specified film thickness and volume flux at each end; only one end of the domain is moving, which is analogous to the upper eyelid moving with each blink. Realistic lid motion from observed blinks is included in the model with end fluxes specified to more closely match the blink cycle than those previously reported. Numerical computations show quantitative agreement with *in vivo* tear film thickness measurements under partial blink conditions. A transition between periodic and non-periodic solutions has been estimated as a function of closure fraction and this may be a criterion for what is effectively a full blink according to fluid dynamics.

Keywords: tear film; blink cycle; partial blinks; lubrication theory; interferometry.

1. Introduction

In this paper, we study two model problems that include many essential elements of the 'blink cycle' that forms the tear film. The blink cycle includes the opening or upstroke of the lids, the time that the lids are open and the closing or downstroke of the lids. Including the downstroke in a model, and thus studying the complete blink cycle, was first carried out by Braun (2006) and Braun & King-Smith (2007). The models generalize this previous work by using realistic lid motion over one or more blink cycles and by incorporating physiological end fluxes necessary for the blink cycle that were previously omitted. An improved numerical method was developed to solve these more general problems as well. We begin with a brief introduction to the tear film, and then describe relevant prior work on tear film drainage.

The human tear film has typically been considered to be a multilayer film that plays a number of roles to maintain the health and function of the eye (Ehlers, 1965; Mishima, 1965). A sketch of a side view of the eye and the overlying tear film are shown in Fig. 1. Mucus is secreted from goblet cells in the epithelium and some of it resides at and above the epithelial cells (Rolando & Refojo, 1983; Sharma *et al.*, 1999); the mucus at the epithelium is thought to be gel-forming mucins that are found among the finger-like bumps, or microplicae, and among long transmembrane mucins that protrude from

†Email: braun@math.udel.edu

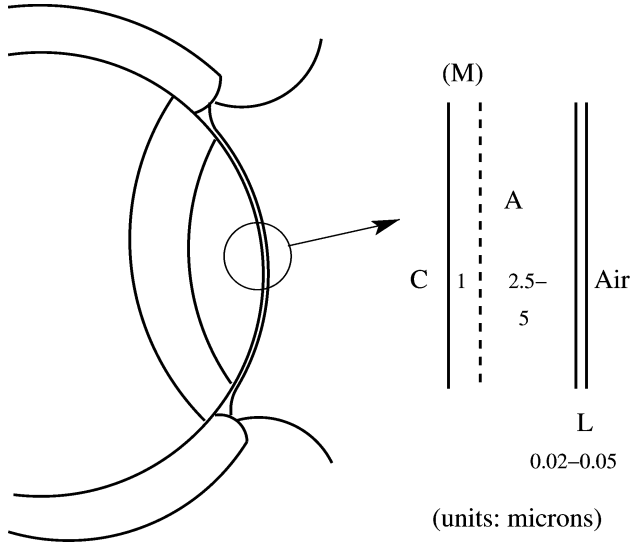

FIG. 1. A sketch of the PCTF. Here, C denotes the cornea, M a possible mucus layer, A the aqueous layer and L the lipid layer. Typical thicknesses are given for each layer in microns. The roles of the lipid and mucus layers will be reduced to appropriate boundary conditions for the aqueous layer. The cornea is modelled as a flat wall because the tear film thickness is so small compared to the radius of curvature of the eye surface after Berger & Corrsin (1974).

those microplicae (Chen *et al.*, 1997; Gipson, 2004; Bron *et al.*, 2004). The surface of these mucins is modelled by a smooth surface for the purposes of fluid dynamic modelling after Braun & Fitt (2003), e.g.

The aqueous layer is primarily water (about 98%, with a variety of components forming the balance) and lies above the cornea and any possible mucus layer (Mishima, 1965; Fatt & Weissman, 1992); the aqueous layer is, essentially, what is commonly thought of as tears. Opinion regarding the amount of mucins that are in the aqueous part of the film has varied over the years, but the three-layer model appears to be acceptable for our purposes here (Bron *et al.*, 2004; Holly, 1973; Holly & Lemp, 1977) though there are soluble gel-forming mucins that play a number of roles in the aqueous layer (Gipson, 2004). It is certainly true that the interface between the aqueous and the mucus layer, if there is a sharp interface, is difficult to observe experimentally as discussed by King-Smith *et al.* (2004). We note that consideration of the mucus film as a separate entity from the other layers of the tear film is still a matter of debate which will not be settled here.

The outermost (lipid) layer is composed of an outer non-polar layer with polar surfactants at the aqueous–lipid interface (McCulley & Shine, 1997; Bron *et al.*, 2004); it decreases the surface tension of, and the evaporation rate from, the air–tear film interface and thus helps stabilize the tear film against rupture ('tear film break-up' in eye literature). In this work, we focus on the evolution of the aqueous layer. Based on the arguments in Braun & Fitt (2003) and references therein, we assume that the mucus–aqueous interface is a flat boundary with hydrodynamic slip while the lipid layer is either ignored or modelled as a deformable, uniformly stretching surface.

There have been a number of theoretical studies of the pre-corneal tear film (PCTF) evolution following a blink, hereafter termed relaxation (Wong *et al.*, 1996; Sharma *et al.*, 1998; Braun & Fitt, 2003; Miller *et al.*, 2003). The common thread among these works is the competition of viscous and capillary forces. All these papers found that reasonable times to rupture were possible in various lubrication models for the thin film evolution and all found t^{α} thinning, with $\alpha = -0.45$ or -0.46, of the thinnest

point in the film (located near the menisci). Braun & Fitt (2003) added the effects of gravitation and evaporation to the evolution during relaxation.

The formation of the tear film was first studied as a coating flow problem by Wong *et al.* (1996), using a quasi-steady analysis that modified the Landau–Levich dip-coating problem (Levich, 1962; Probstein, 1994). Both the formation and the relaxation of an already formed film were studied by Wong *et al.* (1996). They predicted reasonable thicknesses in the micron range from their theory; the approach was later used to derive tear film thicknesses from meniscus radius measurements (Creech *et al.*, 1998), and a wide range of values were found with the latter approach. More recent work analysing the tear film volume suggested that this theory may be insufficient to spread the tear film without a supply of tear film from under the lids (King-Smith *et al.*, 2004).

Models for tear film formation were significantly advanced by Jones *et al.* (2005); they developed a lubrication model that allowed the combined study of film formation and relaxation. Two models were formulated for the deforming air–tear interface of the tear film: a clean interface (assumes a pure tear fluid) and an uniform stretching model of the interface (resulting from a strong insoluble surfactant). Their models had a moving end (corresponding to the upper eyelid), and they found results for the opening and subsequent relaxation within a single blink cycle. Model fluxes from the moving end were included to approximate tear supply from the upper eyelid. They found that no-flux conditions did not allow sufficient coverage of the underlying surface and that a flux of tear fluid from the eyelids was needed to provide adequate coverage; this supported the analysis of King-Smith *et al.* (2004). Furthermore, they verified that in most cases, the piecewise parabolic initial conditions often used in tear film relaxation calculations produced results quite similar to those where the film was generated from a blink and then allowed to relax.

In Braun (2006) and Braun & King-Smith (2007), the blink cycle was studied in which the tear film is repeatedly reformed. This work extended that of Jones *et al.* (2005) by including closing as well as opening in their two models, but a simplified sinusoidal lid motion was used. For the blink cycle, it was found that the lid need not close completely for periodic solutions to occur. A periodic solution for the film was interpreted to mean that blink was effectively a full blink with regard to the fluid dynamics of the tear film. In Braun & King-Smith (2007), a comparison was made between the quantitative *in vivo* pre-lens tear film (PLTF) thickness measurements and the computed results from partial (half) blinks. The computed results showed a pronounced valley as did the *in vivo* tear film, but the computed results from the simplified lid motion were too thick compared to the real film.

In this work, we incorporate realistic lid motion functions that fit observed lid motion data (Doane, 1980; Berke & Mueller, 1998) into two fluid dynamic models for the tear film, and do this for multiple blink cycles. We generalize the flux boundary conditions developed by Jones *et al.* (2005) as an initial step towards implementing the theory of tear film drainage proposed by Doane (1981) for the blink cycle. We compare the results with quantitative *in vivo* tear film thickness measurements made after a half blink for a PLTF. We believe that the comparison is better when we incorporate previously unused fluxes due to supply from the lacrimal gland and drainage through the puncta into the lacrimal drainage system.

We begin with the problem formulation in Section 2, then present results in Section 4, followed by discussion and conclusion in Sections 5 and 6.

2. Formulation

A sketch of the mathematical model for the tear film is shown in Fig. 2. The coordinate directions (x', y') and velocity components (u', v') are along and perpendicular to the flat surface that approximates the corneal surface; primes denote dimensional variables. The scalings are as follows: $L' = 5$ mm is half the

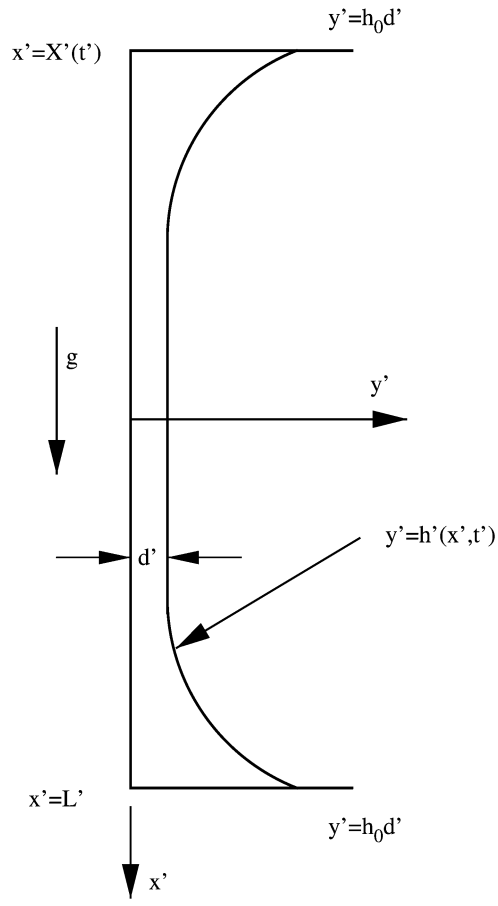

FIG. 2. A sketch of the PCTF indicating important mathematical quantities. The dimensional upper lid location is $X'(t')$; this end executes periodic motion in blink cycle models. For post-blink models (Wong *et al.*, 1996; Sharma *et al.*, 1998; Braun & Fitt, 2003; Miller *et al.*, 2003), the end remains fixed at $X'(t') = -L'$.

width of the palpebral fissure and is used in the x-direction; the characteristic thickness of the tear film away from the ends is $d' = 5$ μm for a tear film. The ratio of the length scales, $\epsilon = d'/L'$, is the small parameter for lubrication theory; for the above scales, $\epsilon \approx 10^{-3}$. The velocity scale along the film is the maximum or mean blink closing speed, $U_{\mathrm{m}} = 10$–30 cm/s for the maximum speed case (Doane, 1980; Berke & Mueller, 1998). ϵU_{m} is the characteristic speed across the film. The timescale is $L'/U_{\mathrm{m}} = 0.05$ s for real blink speeds. We will use the following properties: the surface tension $\sigma_0 = 45$ mN/m, the density $\rho = 10^3$ kg/m^3, the viscosity $\mu = 10^{-3}$ Pa·s and $g = 9.81$ m/s^2. The subscript 0 indicates evaluation at a reference value; in this case, we view it as the fully open state with lowest average surface concentration. The pressure p is made non-dimensional with the viscous scale $\mu U_{\mathrm{m}}/(d'\epsilon)$.

Non-dimensionalization results in the leading-order parallel flow problem on $0 \leqslant y \leqslant h(x, t)$:

$$u_x + v_y = 0, \quad u_{yy} - p_x + G = 0 \quad \text{and} \quad p_y = 0. \tag{2.1}$$

The equations are for mass conservation and momentum conservation in the x- and y-directions, respectively. The inertial terms in the x-component of momentum conservation are proportional to $\epsilon\mathrm{Re}$, where

$\mathrm{Re} = \rho U_\mathrm{m} d'/\mu$ is the Reynolds number; using the small value of U_m, $\mathrm{Re} \approx 1$ making the factor $\epsilon\mathrm{Re}$ small and so we neglect it. The inertial terms in the other momentum equation, compared to an O(1) pressure gradient, are proportional to $\epsilon^3\mathrm{Re}$ and the viscous terms are $\mathrm{O}(\epsilon^2)$ or smaller. Here,

$$G = \frac{\rho g (d')^2}{\mu U_\mathrm{m}} \tag{2.2}$$

is the Stokes number. For typical blink conditions and normal tear film thicknesses, $G \approx 2.5 \times 10^{-3}$. The small Stokes number means that one will have to compute for long times to see any significant effect of gravity under normal blink conditions; results of Jones *et al.* (2005) illustrated this fact and once the evolution equations are derived, we will neglect it in this paper.

On the impermeable wall at $y = 0$, we have the boundary conditions

$$u = \beta u_y, \quad v = 0; \tag{2.3}$$

the first condition is the Navier slip condition and the second is impermeability. Here, $\beta = L_\mathrm{s}'/d'$ is the slip coefficient where L_s' is the slip length; this parameter was discussed in Braun & Fitt (2003) with $10^{-3} \leqslant \beta \leqslant 10^{-2}$. One may also argue that the size of L_s' is based on a molecular length scale, and perhaps the largest size is that of membrane-bound mucins at about 0.3 μm; using this scale gives $\beta \approx 10^{-1}$ but this is likely too large for the tear fluid. Using the size of water molecules gives a much smaller β but this ignores any mucin effect. The slip condition is required to relieve a stress singularity at the junction of the lid with the eye surface if the eyelid is assumed to act as a 'windshield wiper' while opening and closing, similar to the problem with a moving contact line. The case can be made that there is a fluid film under the moving lid that prevents a singularity from the putative surface of the cornea (Jones *et al.*, 2005; Huh & Scriven, 1971), but there still may be slip at the surface of the eye (Zhang *et al.*, 2003) due to the complex surface there (Gipson, 2004; Bron *et al.*, 2004). We assume that values of slip for the PCTF at the corneal surface are near the large end of the available range in alignment with the latter authors, and we choose to include slip in an attempt to model this surface more closely. For the PCTF, we choose $\beta = 10^{-2}$ unless otherwise noted. In Section 4.1.1, we explore the consequences of varying this parameter, and for comparison with the *in vivo* PLTF for which good data are available, we reduce this value to $\beta = 10^{-3}$. We do not include any intermolecular or van der Waals forces here; they will be treated in a future paper.

At the free surface, we have the kinematic and stress conditions

$$h_t + u h_x = v, \quad p = -S h_{xx} \quad \text{and} \quad u_y = M \Gamma_x, \tag{2.4}$$

where

$$S = \frac{\epsilon^3}{\mathrm{Ca}} = \frac{\epsilon^3 \sigma_0}{\mu U_\mathrm{m}}, \quad M = \left(\Gamma \frac{\partial \sigma}{\partial \Gamma}\right)_0 \frac{\epsilon}{\mu U_\mathrm{m}} = \frac{\hat{M}}{\epsilon} \tag{2.5}$$

and $\mathrm{Ca} = \mu U_\mathrm{m}/\sigma_0$. For the lowest maximum speed, we find $\mathrm{Ca} \approx 2 \times 10^{-3}$ and $S \approx 5 \times 10^{-7}$; these values are appropriate for a full blink, but larger S values may be appropriate for partial blinks. Here, $\Gamma = \Gamma(x, h, t)$ is the surface concentration of a polar component of the lipid layer at the lipid–aqueous surface, this is what we mean by the surfactant on the free surface. We estimate that $(\Gamma \partial\sigma/\partial\Gamma)_0 = 0.01$ N/m, and using real blink parameters, we estimate $\hat{M} = 10^{-4}$ and $M = 0.1$. This is a significant value for the Marangoni effect that is plausible in comparison with ocular surface observations (Berger & Corrsin, 1974; Owens & Phillips, 2001). The surface concentration of a polar component of the lipid

layer at the lipid–aqueous interface is governed by the transport equation

$$\Gamma_t + (u^{(s)}\Gamma)_x = P^{-1}\Gamma_{xx}. \tag{2.6}$$

Here, $u^{(s)}$ is the surface velocity, $P^{-1} = D/L'U$ is the Péclet number and D is the surface diffusivity of Γ. With $D = 10^{-9}$ m^2/s, we estimate $P^{-1} \approx 2 \times 10^{-6}$; thus, diffusion of surfactant is small during the blink itself and is neglected in this paper.

The two cases of this paper differ in the treatment of the tangential stress boundary condition. In one case, the film is treated as a pure liquid with a clean surface in contact with a passive gas; then $M = 0$ and the surfactant transport equation is decoupled from the evolution. Let the approximate velocity component in the x-direction be $u^{(1)}$ in this case. In the other case, the pure fluid has an insoluble surfactant at its interface with the passive gas, and the effect on the surface tension is so strong that the surface responds in a manner that is analogous to, but not the same as, the tangentially immobile case when the domain length is fixed. Let the approximate horizontal velocity component in this case be $u^{(2)}$. The flux of fluid across any cross-section of the film in these respective cases is then

$$q^{(i)} = \int_0^h u^{(i)}(x, y, t)\mathrm{d}y, \quad i = 1, 2. \tag{2.7}$$

Jones *et al.* (2005) called these limits the inactive and active lipid layers, respectively; we prefer the terms stress-free limit (SFL) and uniform stretching limit (USL). A mathematical derivation of the latter limit has been included in Appendix A (Braun, 2006; Braun & King-Smith, 2007).

In either case, using the kinematic condition and mass conservation, the free surface evolution is given by

$$h_t + q_x^{(i)} = 0 \quad \text{on } X(t) \leqslant x \leqslant 1. \tag{2.8}$$

For the SFL, we obtain

$$q^{(1)} = (Sh_{xxx} + G)\left(\frac{h^3}{3} + \beta h^2\right); \tag{2.9}$$

in the USL, we obtain

$$q^{(2)}(x, t) = \frac{h^3}{12}\left(1 + \frac{3\beta}{h + \beta}\right)(Sh_{xxx} + G) + X_t\frac{1 - x}{1 - X}\frac{h}{2}\left(1 + \frac{\beta}{h + \beta}\right). \tag{2.10}$$

Note that for the USL case, if $X_t = 0$, we recover the equation for the free surface with slip on the bottom surface but a large M free surface. If $\beta = 0$ as well, we recover the tangentially immobile case with a no-slip bottom surface. As noted above, we only present results with $G = 0$ in this work.

2.1 *Lid motion*

The domain along the eye surface varies during a blink; we denote it by $X'(t') \leqslant x \leqslant L'$ as indicated in Fig. 2. The location of the upper lid is specified by $X'(t')$ (prime indicates dimensional quantity); the lower lid is always at $L' = 5$mm. A mathematical fit to the lid position at the centre of the palpebral fissure (eye opening) was obtained by Berke & Mueller (1998) for the data in Berke & Mueller (1996); comparison was made with similar data of Doane (1980). Blink data were also measured and fit by Jones *et al.* (2005). We note that Doane (1980) discusses the difficulty of obtaining data for unforced blinks,

and fits from blinks where the subject is conscious of being observed will likely result in motions subtly modified from unforced blinks.

We describe the lid motion in two stages; first, complete blink motion is specified. In the second, incomplete closure is described; it is the latter that we shall use in all computations in this paper.

2.1.1 *Full lid closure.* The relations given by Berke & Mueller (1998) are repeated below in terms of the coordinate system of our previous work (Braun, 2006; Braun & King-Smith, 2007) where the origin is the middle of the fully open domain (when $X'(t') = -L'$). Thus, the domain at any time is given by $X'(t') \leqslant x' \leqslant L'$ for complete closure. When the lid is closing,

$$X'(t') = -L' + 2L'(t'/\Delta t'_{\rm oc})^2\, {\rm e}^{[1-(t'/\Delta t'_{\rm oc})^2]} \tag{2.11}$$

for $0 \leqslant t' \leqslant \Delta t'_{\rm oc}$ with the time interval for closing given by $\Delta t'_{\rm oc} = 0.0821$ s. During opening,

$$X'(t') = L' - 2L'\left(\frac{t' - \Delta t'_{\rm oc}}{\Delta t'_{\rm co}}\right)^2 \exp\left[1 - \left(\frac{t' - \Delta t'_{\rm oc}}{\Delta t'_{\rm co}}\right)^2\right] \tag{2.12}$$

for $\Delta t'_{\rm oc} \leqslant t' \leqslant \Delta t'_{\rm oc} + \Delta t'_{\rm co}$ with the upstroke occuring in the time interval $\Delta t'_{\rm co} = 0.1758$ s. The balance of the duration of a blink cycle, $\Delta t'_{\rm oc} + \Delta t'_{\rm co} \leqslant t' \leqslant \Delta t'_{\rm bc}$, has $X'(t') = -L'$. Here, $\Delta t'_{\rm bc} = \Delta t'_{\rm oc} + \Delta t'_{\rm co} + \Delta t'_{\rm o}$ is the duration of the entire blink cycle and $\Delta t'_{\rm o}$ is the interblink period within the blink cycle; we will assume an interblink period of 5 s. This interblink time is a reasonable value at the short end of an acceptable range.

2.1.2 *Non-dimensional incomplete closure.* According to Doane (1980) and Berke & Mueller (1998), many blinks are incomplete, i.e. the lids do not fully close. This is a useful situation to begin modelling the fluid dynamics of the full blink process. Let the lids be separated by a distance $2\lambda L'$ at the end of the closing part of the blink, where λ is the fraction of the fully open eye width. Then, the upper lid position moves between $-L' \leqslant X'(t') \leqslant L'(-2\lambda + 1)$; rearranging the blink motion so that the cycle begins at the closed position and non-dimensionalizing with $x = x'/L'$ give

$$X(t) = \begin{cases} 1 - 2\lambda - 2(1-\lambda)\left(\frac{t}{\Delta t_{\rm co}}\right)^2 \exp\left[1 - \left(\frac{t}{\Delta t_{\rm co}}\right)^2\right], & 0 \leqslant t \leqslant \Delta t_{\rm co}, \\ -1, & \Delta t_{\rm co} \leqslant t \leqslant \Delta t_{\rm co} + \Delta t_{\rm o}, \\ -1 + 2(1-\lambda)\left(\frac{t - \Delta t_{\rm co} - \Delta t_{\rm o}}{\Delta t_{\rm oc}}\right)^2 \exp\left[1 - \left(\frac{t - \Delta t_{\rm co} - \Delta t_{\rm o}}{\Delta t_{\rm oc}}\right)^2\right], & \Delta t_{\rm co} + \Delta t_{\rm o} \leqslant t \leqslant \Delta t_{\rm bc}. \end{cases} \tag{2.13}$$

Here, $\Delta t_{\rm bc} = \Delta t_{\rm co} + \Delta t_{\rm o} + \Delta t_{\rm oc}$ is the non-dimensional period of the complete blink cycle. The lid motion is now on the interval $-1 \leqslant X(t) \leqslant 1 - 2\lambda$ and the tear film is on the interval $X(t) \leqslant x \leqslant 1$. When non-dimensionalized based on $L' = 5$ mm and $U_{\rm m} = 10$ cm/s, the duration of the upstroke is $\Delta t_{\rm co} = 3.52$; for the downstroke, $\Delta t_{\rm oc} = 1.64$, and for the interblink time, $\Delta t_{\rm o} = 100$. Thus, the blink cycle duration is $\Delta t_{\rm bc} = 105.16$.

2.2 *Flux conditions at the boundary*

The fluxes model the flow along the lids during the blink cycle as described by Doane (1981). We note that there are limitations to approximating the drainage flow and the influx of tear fluid at a single point

at the end of the film, but the system is sufficiently complicated that we are satisfied to begin with this level of modelling. The flux conditions are

$$q^{(i)}(X(t),t) = X_t h_0 + Q_{\text{top}} \quad \text{and} \quad q^{(i)}(X(t),t) = -Q_{\text{bot}}, \tag{2.14}$$

where Q_{top} and Q_{bot} are the respective fluxes into the domain at the moving and stationary ends.

2.2.1 *Flux proportional to lid motion.* Jones *et al.* (2005) used the following flux functions (when non-dimensionalized in our scales):

$$Q_{\text{top}} = -X_t h_e \quad \text{and} \quad Q_{\text{bot}} = 0, \tag{2.15}$$

with $h_e = h'_e/d'$ chosen to supply the correct amount of fluid from under the upper lid during the upstroke of the blink (note that $X_t < 0$ in the upstroke). We designate this set of flux boundary conditions as flux proportional to lid motion (FPLM). In Jones *et al.* (2005), $h'_e = 8.24$ μm. This choice was based on estimated tear film thickness under the lower lid from a paper by Norn (1966); in that paper, a small section of fluid was extracted using a micropipette after holding back the lower lid and that thickness was doubled to estimate 7.8 μm of tear film. However, Jones *et al.* (2005) based their computations on a 10-μm tear film, whereas we are expecting a 5-μm film or less. Also, there is evidence that the tear film thickness under the lids is smaller at the margin from X-ray tomography (Kessing, 1967). Given these last two points, we believe that we must pick h'_e smaller than 8.24 μm.

In some cases, we choose to use a similar proportion of tear film fluid arriving from under the lids, and thus for the 5-μm film, e.g. we may choose $h'_e = 4$ μm, and non-dimensionally we find $h_e = h'_e/d' = 0.8$. Now, the added volume during the upstroke of the blink is

$$\Delta V = \int_0^{\Delta t_{\text{co}}} -X_t h_e \, \mathrm{d}t = -\, h_e X|_0^{\Delta t_{\text{co}}} = -h_e\,[-1-(1-2\lambda)] = h_e(2-2\lambda). \tag{2.16}$$

In our dimensionless variables, the corresponding initial volume is $V_i = V_0 - 2(1-\lambda)h_e$, where we choose $1.376 \leqslant V_0 \leqslant 2.576$ and $0.25 \leqslant h_e \leqslant 0.8$. The larger end of the volume range comes from estimating the volume for a $d' = 5$ μm film with quadratic menisci having width 0.36 mm and height $h_0 d'$ at both ends. The smaller end of the volume range is meant to simulate a reduced tear volume, corresponding to a 2.0-μm thick film away from the menisci (found by subtracting a uniform thickness of 0.6 from the former number). An example of the FPLM boundary conditions is shown in Fig. 3.

2.2.2 *Lacrimal gland and punctal drainage fluxes.* We explore FPLM boundary conditions for some cases here, but these boundary conditions do not take into account the action of the puncta, which cause a significant drainage along the lid margins beginning with the lids about halfway open or so and ends up to 3 s after the lids have fully opened (Doane, 1981). We pose Gaussian functions for both the punctal fluxes and the influx of new tear fluid from the lacrimal gland. For conserving the total volume over a cycle, the following flux functions are used for a 'full' blink. The flux function for the upper lid is

$$Q_{\text{top}} = -2\, f_{\text{out}} Q_{0\text{p}} \exp\left[-\left(\frac{t-t_{\text{out}}}{\Delta t_{\text{p}}}\right)^2\right] + f_{\text{top}} Q_{0\text{lg}} \exp\left[-\left(\frac{t-t_{\text{in}}}{\Delta t_{\text{co}}/2}\right)^2\right], \tag{2.17}$$

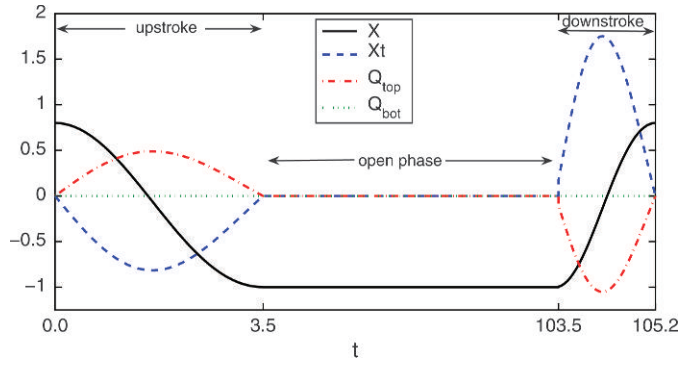

FIG. 3. An example of the lid motion $X(t)$, lid speed $X_t(t)$ and boundary fluxes $Q_{\text{bot}} = 0$ and $Q_{\text{top}} = -X_t h_e$ with $\lambda = 0.1$ for FPLM boundary conditions. Note that the t axis is not to scale.

and for the bottom,

$$Q_{\text{bot}} = -2(1 - f_{\text{out}})Q_{0\text{p}} \exp\left[-\left(\frac{t - t_{\text{out}}}{\Delta t_{\text{p}}}\right)^2\right] + (1 - f_{\text{top}})Q_{0\text{lg}} \exp\left[-\left(\frac{t - t_{\text{in}}}{\Delta t_{\text{co}}/2}\right)^2\right]. \tag{2.18}$$

The terms proportional to $Q_{0\text{lg}}$ represent supply of tear fluid from the lacrimal gland and those proportional to $Q_{0\text{p}}$ represent the opening and filling of the puncta as part of the lacrimal drainage system (Doane, 1981). f_{top} interpolates the influx between the top and the bottom, with unity allowing influx only at the top; we typically use $0.6 \leqslant f_{\text{top}} \leqslant 0.75$. Assigning most influx of new tear fluid from the upper lid seems reasonable due to the critical nature of the lacrimal gland in tear film secretion (Lorber, 2007) and from tear film observations (Maurice, 1973; Doane, 1981). The factor f_{out} keeps drainage of tear fluid from the film evenly split when its value is 0.5, and we may consider values in the interval [0,1]; typically, we used $0.5 \leqslant f_{\text{out}} \leqslant 0.65$ here. We now discuss our choices for the magnitudes and duration of these contributions to the fluxes at the ends of the films.

For the lacrimal gland supply, we wish to match the estimated steady supply from the lacrimal gland of 1.2 μl/min (Mishima *et al.*, 1966); the corresponding non-dimensional flux is $Q_{mT} = 0.01$ when referred to $U_{\text{m}} d' L'$. To compute $Q_{0\text{lg}}$, we need the integral of the influx term over a complete cycle to balance the average influx; mathematically,

$$Q_{0\text{lg}} \int_{-\Delta t_{\text{bc}}/2}^{\Delta t_{\text{bc}}/2} \mathrm{e}^{-(t - t_{\text{in}})^2/(\Delta t_{\text{co}}/2)^2} \, \mathrm{d}t = Q_{mT} \Delta t_{\text{bc}}. \tag{2.19}$$

We can approximate the integral of the Gaussian by taking an infinite domain to arrive at

$$Q_{0\text{lg}} = \frac{w_{\text{in}}}{\sqrt{\pi}} \frac{\Delta t_{\text{bc}}}{\Delta t_{\text{co}}} Q_{mT}. \tag{2.20}$$

This tear fluid is supplied during the upstroke of the blink cycle, over a time span of about $4\Delta t_{\text{co}}$. For $\Delta t_{\text{o}} = 100$, we obtain $Q_{0\text{lg}} = 0.337$ and if $\Delta t_{\text{o}} = 20$, we find $Q_{0\text{lg}} = 0.0805$. Having $f_{\text{top}} < 1$ allows for some influx from the bottom; this is possible physiologically because the inferior and superior menisci communicate via the canthus (Maurice, 1973), and there are also relatively small lacrimal glands in the lower lid as well (Lorber, 2007).

For the punctal drainage terms, we choose the amplitude to match the amount supplied from the lacrimal gland. Thus, the integral of the drainage term must equal that from the lacrimal gland yielding the relation

$$Q_{0\mathrm{p}} = \frac{1}{2\sqrt{\pi}} \left(\frac{\Delta t_{\mathrm{bc}}}{\Delta t_{\mathrm{co}}} \right) Q_{mT} = \frac{1}{4} \left(\frac{\Delta t_{\mathrm{co}}}{\Delta t_{\mathrm{p}}} \right) Q_{0\mathrm{lg}} \tag{2.21}$$

when this drainage is evenly split between the top and the bottom lids. We use the value $Q_{0\mathrm{p}} = 0.0297$.

For the remaining parameters in the flux, we make the following choices, unless otherwise indicated: $t_{\mathrm{out}} = 2\Delta t_{\mathrm{p}} + \Delta t_{\mathrm{co}}/2$ and $\Delta t_{\mathrm{p}} = 10$. Here, t_{out} is the time of the peak outflux component for either end. With these choices of parameters, the punctal drainage is over in 2 s after the lid opens, in accord with observations (Doane, 1981; Maurice, 1973).

We make these functions smooth at the end of a blink cycle by adding terms that have been shifted by Δt_{bc}, the length of one blink cycle.

2.2.3 *Combining FPLM, lacrimal influx and punctal outflux.* We now superimpose the FPLM and the Gaussian fluxes from the lacrimal glands and drainage into the puncta in an effort to obtain more realistic boundary conditions; this case will be designated FPLM+ boundary conditions. For the moving end, Q_{top} is found by superimposing the fluxes from (2.15) and (2.17). In this case, we should view h_e as adjustable, and we vary it over the interval $0.2 \leqslant h_e \leqslant 0.8$. Note that the initial volume V_i still varies when h_e is varied as above. The effect of this is to vary the distribution of the tear film between the exposed and the unexposed portions in the initial state as well as vary how much gets exposed by the lid gliding over unexposed film. For the bottom lid, the flux remains the same as in (2.18).

An example of FPLM+ boundary conditions is shown in Fig. 4; this case corresponds to Fig. 3 with the same intervals for the upstroke, open phase and downstroke. Finally, the fluxes were chosen to be in phase due to the expected simultaneous opening of the canaliculi in the blink process in eyes (Doane, 1981). The addition of an outflux from the ends due to the puncta and influx due the lacrimal gland is a new component of the modelling which was not present in that of Jones *et al.* (2005) and it represents a step towards constructing models of Doane's (1981) theory of drainage during the blink cycle.

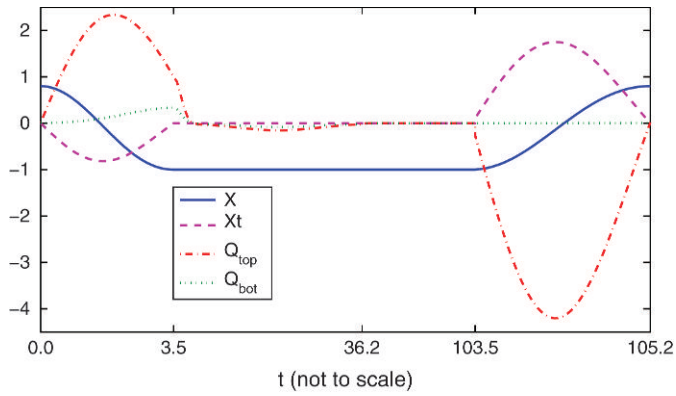

FIG. 4. An example of the lid motion $X(t)$, lid speed $X_t(t)$ and boundary fluxes Q_{bot} and Q_{top} with $\lambda = 0.1$ for FPLM+ boundary conditions. The lacrimal gland supply is approximated with $Q_{0\mathrm{lg}}$ given by (2.20), matching the 1.2-μl/min average flux and the punctal drainage flux given by (2.21) to conserve the tear volume over the blink cycle.

2.3 *Domain mapping and initial condition*

For the purposes of numerical solution, we find it convenient to transform the domain $X(t) \leqslant x \leqslant 1$ to a fixed domain $-1 \leqslant \xi \leqslant 1$ via

$$\xi = 1 - 2\frac{1-x}{1-X(t)}. \tag{2.22}$$

Using the changes of variable $h(x,t) = H(\xi(t),t)$ and $q^{(i)}(x,t) = Q^{(i)}(\xi,t)$, the derivatives in the evolution equations are modified as follows:

$$h_t = H_t - H_\xi X_t \frac{1-\xi}{1-X}, \quad h_x = H_\xi \frac{2}{1-X}, \quad h_{xx} = H_{\xi\xi}\left(\frac{2}{1-X}\right)^2, \text{ etc.} \tag{2.23}$$

The initial condition is most easily specified in terms of these new variables. We use the polynomial initial condition

$$H(\xi,0) = H_{\min} + (h_0 - H_{\min})\xi^m; \tag{2.24}$$

this initial shape is applied when the domain is at its shortest, and the computation starts from this 'closed' state. Typically, $m = 4$ is used, but larger m may be used; values from $m = 2$ to 16 have been tested. Integrating this expression over $-1 \leqslant \xi \leqslant 1$ and equating the result to a desired area determine $H_{\min}$. This initial condition was used in both models.

3. Numerical methods

Because our experience indicates that imposing boundary conditions for the fluxes (2.9) and (2.10) through direct manipulation of the variable H leads to instability and unreasonably small time steps, we first rewrite the partial differential equation (PDE) into the semi-explicit differential algebraic form of index 1 where the flux is considered to be a dependent variable in the PDE system. For the USL, the equations on a fixed domain are

$$H_t = \frac{1-\xi}{1-X}X_t H_\xi - \left(\frac{2}{1-X}\right)Q^{(2)}_\xi, \tag{3.25}$$

$$0 = X_t\frac{1-\xi}{2}\frac{H}{2}\left(1+\frac{\beta}{H+\beta}\right) + \frac{H^3}{12}\left(1+\frac{3\beta}{H+\beta}\right)\left[S\left(\frac{2}{1-X}\right)^3 H_{\xi\xi\xi}\right] - Q^{(2)}, \tag{3.26}$$

$$H(\pm 1,t) = h_0, \quad Q^{(2)}(1,t) = -Q_{\text{bot}}, \quad Q^{(2)}(-1,t) = X_t h_0 + Q_{\text{top}}, \tag{3.27}$$

$$H(\xi,0) = H_{\min} + (h_0 - H_{\min})\xi^m. \tag{3.28}$$

Note that in this form, the boundary conditions do not contain higher derivatives, which aids in obtaining accurate solutions.

For the stress-free case, we replace $Q^{(2)}$ everywhere in the above system with $Q^{(1)}$, where

$$Q^{(1)} = S\left(\frac{2}{1-X}\right)^3\left(\frac{H^3}{3} + \beta H^2\right)H_{\xi\xi\xi}; \tag{3.29}$$

this last relationship replaces the second equation in the system above.

We used three numerical methods in the course of this investigation; all were implementation of the method of lines. Spatial discretizations were used while time was left continuous, then the resulting differential algebraic equations (DAEs) or ordinary differential equations (ODEs) solved using available software; in all cases, we used ode15s in MATLAB to solve the equations after spatial discretization.

In discretized form, H and $Q^{(i)}$ are each $(N+1)$-dimensional vectors:

$$H = \begin{bmatrix} h_0 \\ H_1 \\ \vdots \\ H_{N-1} \\ h_0 \end{bmatrix}, \quad Q^{(i)} = \begin{bmatrix} X_t h_0 + Q_{\text{top}} \\ Q_1^{(i)} \\ \vdots \\ Q_{N-1}^{(i)} \\ -Q_{\text{bot}} \end{bmatrix}, \tag{3.30}$$

where $H_j = H(\xi_j, t)$ and $Q_j^{(i)} = Q^{(i)}(\xi_j, t)$; the grid points ξ_j, $i = 0, \ldots N$, are on the interval $\xi \in [-1, 1]$. Approximation of kth partial derivatives of $H(\xi, t)$ and $Q^{(i)}(\xi, t)$ with respect to ξ can be written as

$$H_{,k} = D^{(k)} H \quad \text{and} \quad Q_{,k}^{(i)} = D^{(k)} Q, \tag{3.31}$$

respectively. The $D^{(k)}$ are the kth-order differentiation matrices and their entries depend on whether the finite difference or the spectral method, to be discussed below, was used. In all the methods of this paper, we impose the boundary conditions $H(\pm 1, t) = h_0$ exactly. Rather than using the flux conditions to find the values of $H_{\xi\xi\xi}(\pm 1, t)$, we use the given boundary data for $Q^{(i)}(\pm 1, t)$ and differentiate the $Q^{(i)}$ vector as needed. This approach worked quite well for stability and for conserving the fluid volume to sufficient accuracy. In a DAE formulation, H_j and $Q_j^{(i)}$, $j = 1, \ldots, N-1$, are unknowns and are solved for by ode15s. In the ODE formulation, only the H_j, $j = 1, \ldots, N-1$, are unknowns and the flux is only computed as an intermediate step in finding the ODEs for the H_j.

We used three different numerical methods in the course of this work. In Method I, the DAE approach was used with finite differences in space. In this method, a uniformly spaced mesh in ξ was used. Centred second-order accurate finite-difference approximations were used for the derivatives inside the domain; non-centred differences were used at the ends. To obtain sufficient accuracy as measured by conservation of volume to within 1%, up to $N - 1 = 4095$ interior grid points were used. This method was used as a baseline for comparison only.

In Method II, the DAE formulation was used with modifications to a Chebyshev spectral collocation for the spatial discretization. We used collocation points that have a minimum spacing of $O(N^{-1})$ by applying a non-symmetric mapping to Chebyshev points. The mapping was developed by Kosloff & Tal-Ezer (1993); two input parameters α and β adjust the locations of the collocation points, and the number of points is slightly increased near the moving end of the domain relative to the stationary end. This approach has two improvements over the typical Chebyshev collocation. First, longer stable time steps are typically allowed; second, the roundoff error is reduced (Don & Solomonoff, 1997). (Further details about the spatial discretization are given in Appendix B and will also appear in Heryudono, 2008.) This method was capable of keeping the error in volume conservation for any results presented here to 10^{-4} or lower over multiple blink cycles, typically using $N - 1 = 379$ collocation points. This result is more accurate than the finite-difference method above, even with a large number of grid points; however, the method was not the most robust in that it could not reach all the parameters we desired.

Method III, the ODE formulation, solves the discretized system (3.25) and (3.26) as a system of ODEs using the same spectral discretization that was used for Method II. This approach allowed us to compute down to $S = 10^{-7}$ in some cases, making this approach significantly more robust than the others, while it maintained essentially the same level of conservation of volume (and thus error) as Method II. While the methods all agree to within their limitations, this last method was used to generate the results appearing in the paper. We also note that neither Method II nor Method III needed any aliasing to perform well.

4. Results

We begin with results from the USL, then move on to the SFL and finish with a comparison with prior film formation results.

4.1 *Uniform stretching limit*

4.1.1 *Full blinks.* We begin with computation of a blink cycle for a full blink with $S = 2 \times 10^{-5}$, $\beta = 10^{-2}$, $V_0 = 2.576$, $\lambda = 0.1$ using FPLM boundary conditions with $h_e = 0.8$. $\lambda = 0.1$ means that only 10% of the film length is left when the eye is closed; the boundary value for the tear film thickness is smaller than for real tear films, but is useful for studying the behaviour in lubrication theory. In this and all cases, $h_0 = 13$. These conditions yield the results shown in Fig. 5. The film is laid down during the upstroke, with the film being thicker towards the moving end (i.e. the top). The evolution of the tear film while the lids remain stationary and fully open results in capillary-driven thinning near the ends matching the results first found by Jones *et al.* (2005). The last panel shows the film evolution during the downstroke of the blink; these results represent part of the new findings in this paper, completing the computation of the full blink cycle with realistic lid motion.

Reducing S to 5×10^{-7} more closely approximates realistic lid speeds; results are shown in Fig. 6 with all other parameters the same. The results are seen to be similar to those for larger S, but there is a more pronounced ripple at the bottom of the moving meniscus for smaller S. While the changes here are not dramatic, we note that the difficulty of such computations increases significantly, and only the spectral ODE formulation can reach this parameter range for the numerical methods used here. Also, there is subtle dependence on S in our results for partial blinks, which will be explored further below.

Varying h_e for $V_0 = 2.576$ gives the results shown in Fig. 7. $h_e = 0.8$ corresponds to the same fraction of the tear film thickness being exposed while the lid opens, as was used in Jones *et al.* (2005); however, we note that our thickness scale is half that of their work. When h_e takes on this larger value, the thickness is larger superiorly (top of the film), as occurs in many cases *in vivo* (Benedetto *et al.*, 1984; King-Smith *et al.*, 2006) and was computed by Jones *et al.* (2005). For smaller values of h_e, the thickness profile flattens and even becomes thicker inferiorly (at the bottom end). In the case of $h_e = 0.4$, the film can be returned to an increased thickness superiorly by using FPLM+ boundary conditions.

Reducing h_e and using FPLM+ boundary conditions yield the results depicted in Fig. 8; here $V_0 = 2.576$, $h_e = 0.4$, $Q_{0\mathrm{lg}} = 0.337$, $Q_{0\mathrm{p}} = 0.0297$, $f_{\mathrm{top}} = 0.75$ and $f_{\mathrm{out}} = 0.65$. There are film thickness profiles shown at the end of the upstroke ($t = 3.52$) and at the end of the open phase ($t = 103.52$, or after 5 s of being open), for both FPLM and FPLM+ boundary conditions. Just after the blink finishes, there is a noticeable difference between the case with FPLM boundary conditions, where the film is essentially flat over the domain, and the case with FPLM+ boundary conditions, where the film is thicker near the

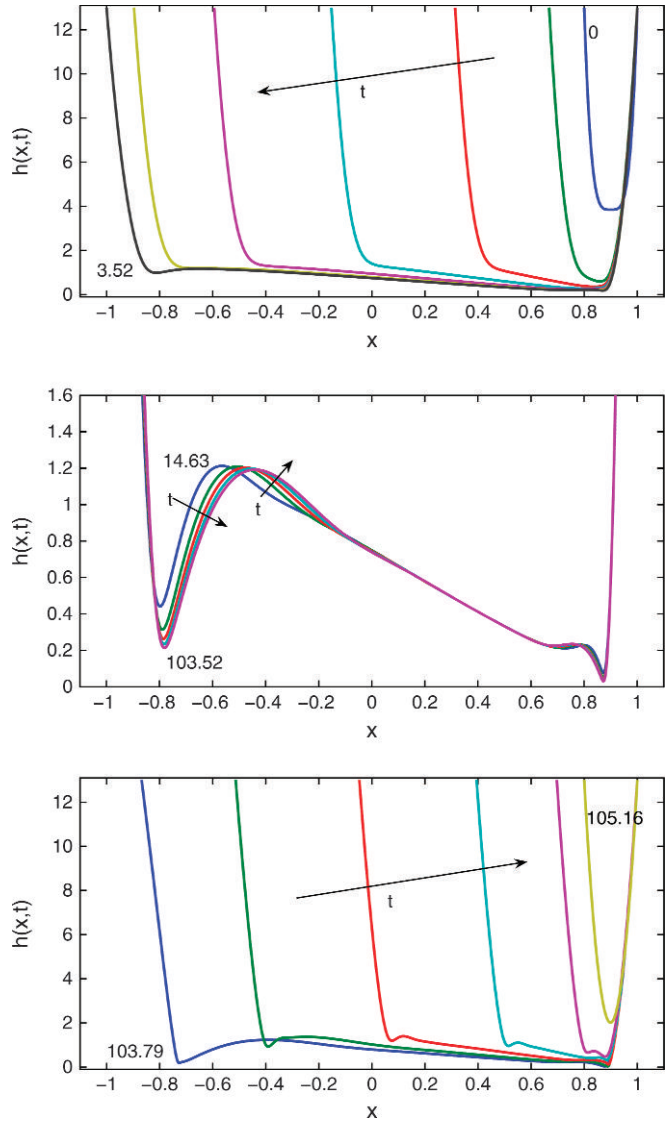

FIG. 5. Top: Upstroke of the blink cycle. Middle: Zoom in the vertical direction for various times while the domain is fully open. Bottom: The downstroke of the blink cycle.

moving end (upper lid). We believe that the latter boundary conditions more accurately represent the thin region of the tear film at its edge by including the action of the lacrimal gland and the puncta. The average supply of tear fluid from the lacrimal gland and the drainage into the puncta were not included in the work of Jones *et al.* (2005), but we believe that they are necessary to study the blink cycle.

For completeness, we explore the effect of slip on the computed solutions. Varying β and using FPLM boundary conditions yield the results depicted in Fig. 9; here $S = 10^{-5}$, $V_0 = 1.576$ and $h_e = 0.4$. For $\beta \leqslant 10^{-2}$, the evidence of slip in the computed solution is not obvious; however, for β on the order of 10^{-1} a region of thinning near the stationary end develops. This occurs because the

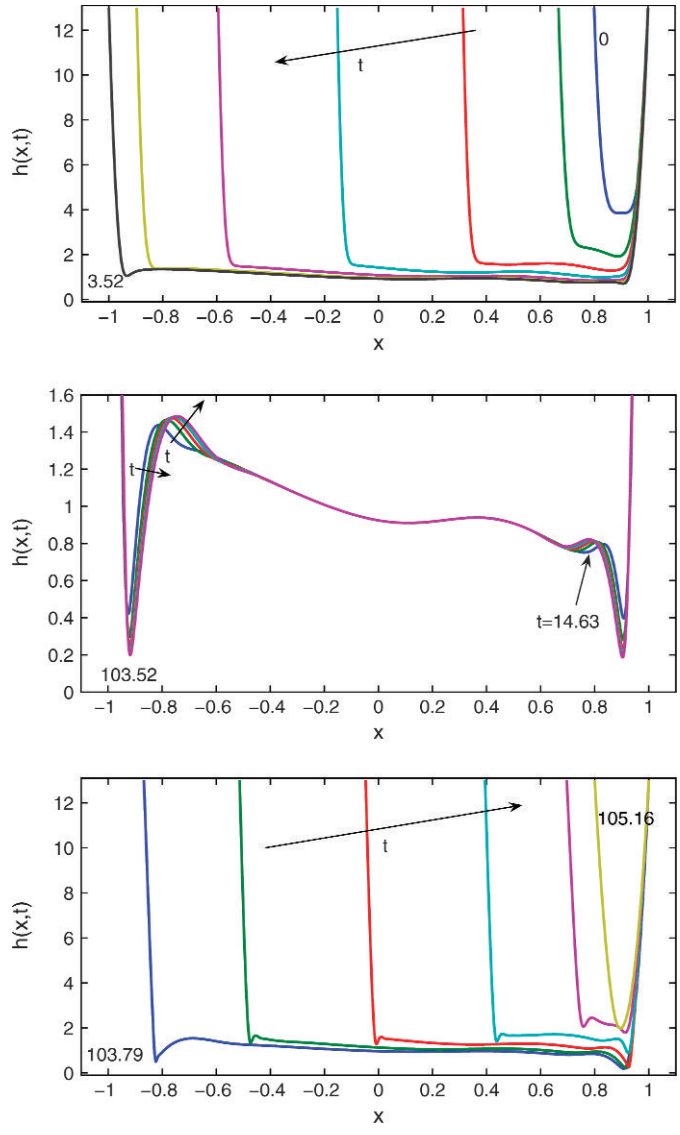

FIG. 6. Same parameters as in Fig. 5 except $S = 5 \times 10^{-7}$. Top: Upstroke of the blink cycle. Middle: Zoom in the vertical direction while fully open. Bottom: The downstroke.

shear stress on the bottom of the film is reduced enough to prevent the 'dragout' of fluid from the moving meniscus. We note that the effects of different sizes of slip have been explored for dewetting by Münch *et al.* (2005); see also references therein. Their work considered dewetting, but they did derive three different models for different sizes of slip: small, intermediate and large. Our computed results correspond to the first two cases; for $\beta \leqslant 10^{-2}$, we compute solutions in the small slip regime. When $\beta > 0.1$, we compute small film sizes near the stationary meniscus and $\beta h^2 > h^3/3$, which corresponds to the intermediate slip regime of their work.

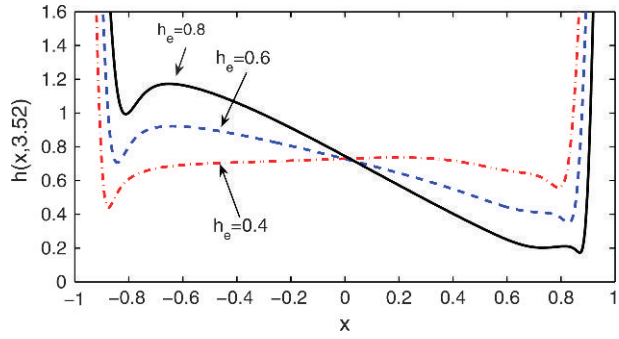

FIG. 7. Film thickness as a function of x while the moving end is fully open with FPLM boundary conditions. h_e is varied from 0.4 to 0.8; the qualitative aspects of the film thickness profile change with this parameter.

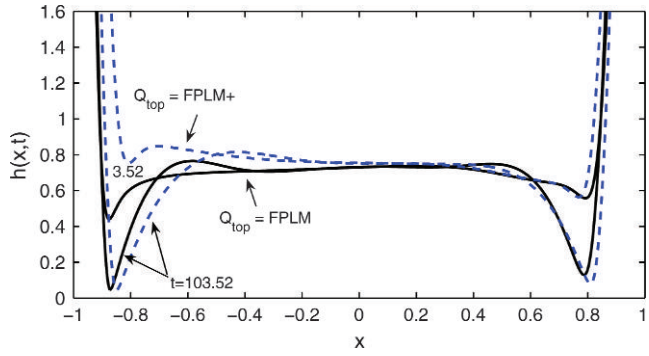

FIG. 8. Film thickness as a function of x for two different times while the ends of the domain are fully extended. The solid line depicts FPLM boundary conditions and the dashed curve represents FPLM+ boundary conditions; in both cases, $h_e = 0.4$. The film can take the expected shape that is thicker superiorly with a reduced thickness exposed from under the lid during blinking.

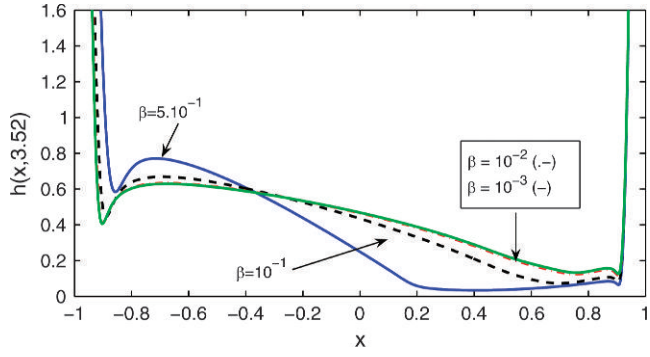

FIG. 9. Film thickness as a function of x for different β when the domain has just become fully extended.

4.1.2 *Partial blinks.* In this section, we study partial blinks. Experimental *in vivo* results are compared quantitatively with computed results from the USL model. We use an example from the PLTF rather than the PCTF because the contrast of interference fringes is considerably higher for the PLTF, making them easier to analyse.

An image of PLTF just after a half blink is shown in Fig. 10. The interference fringes shown in the photo indicate a change of 0.16 μm for each change from light to dark. Thickness data were evaluated along the vertical line just to the left of centre in the figure; these thicknesses are shown as dots in the following figures. We note that the ends of the film (in particular, the menisci and neighbouring thin regions) are not included in that comparison because they are not captured in the photo. The image shown in Fig. 10 was obtained with a light source having a narrow spectral bandwidth, with a consequence that fringe contrast is almost independent of tear film thickness (King-Smith *et al.*, 1999). Simultaneously, a broad spectral bandwidth image (not shown) was obtained, in which the contrast varies inversely with thickness (King-Smith *et al.*, 2006). Thus, absolute thickness at any fringe could be obtained from the ratio of contrasts of broad- and narrow-band images; e.g. the minimum thickness along the vertical line in Fig. 10 was found to be about 0.48 μm.

The curving feature near the left edge of the illuminated region is the edge of the optic zone of the lens. There is a change in lens surface slope at the edge of the optic zone (typically a 3 mm radius), where the shape of the lens changes from optical requirements for improved vision to mechanical requirements for comfort and durability (outside radius of 6 or 7 mm). In this case, the fringes are consistent with the presence of a ridge in the lens at the edge of the optic zone.

The USL simulation begins with a 10% open film ($\lambda_0 = 0.1$), fully opens and then repeats opening and closing with $\lambda = 0.5$. This mimics the upper lid sequence from which Fig. 10 was obtained. The parameters for the first case are $S = 5 \times 10^{-6}$, $\beta = 10^{-3}$, $f_{\text{top}} = 0.6$ and $f_{\text{out}} = 0.55$ for FPLM boundary conditions; results are shown in Fig. 11. In all cases, the measured data are shifted to visually

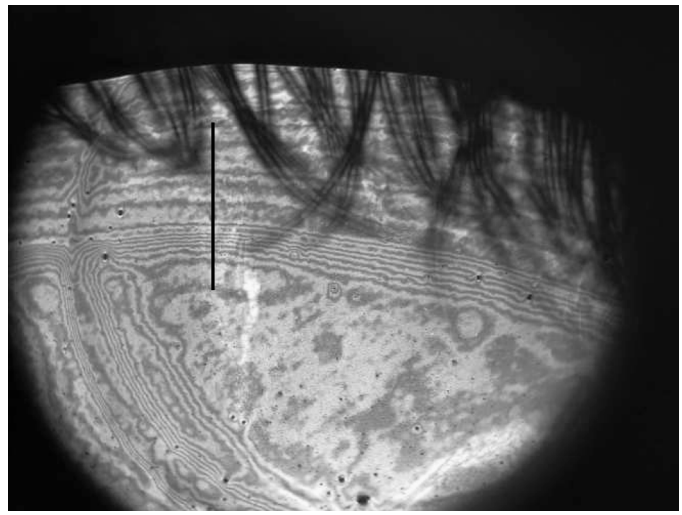

FIG. 10. Interference fringes for the total tear film thickness of the PLTF just after a half blink. The upper lid descended to the region of compact fringes in the middle of the image and then rose to the open position (upper lashes still visible). *In vivo* thickness data were evaluated along the black line. The curving feature near the left edge of the illuminated region is the edge of the optic zone of the lens (see text).

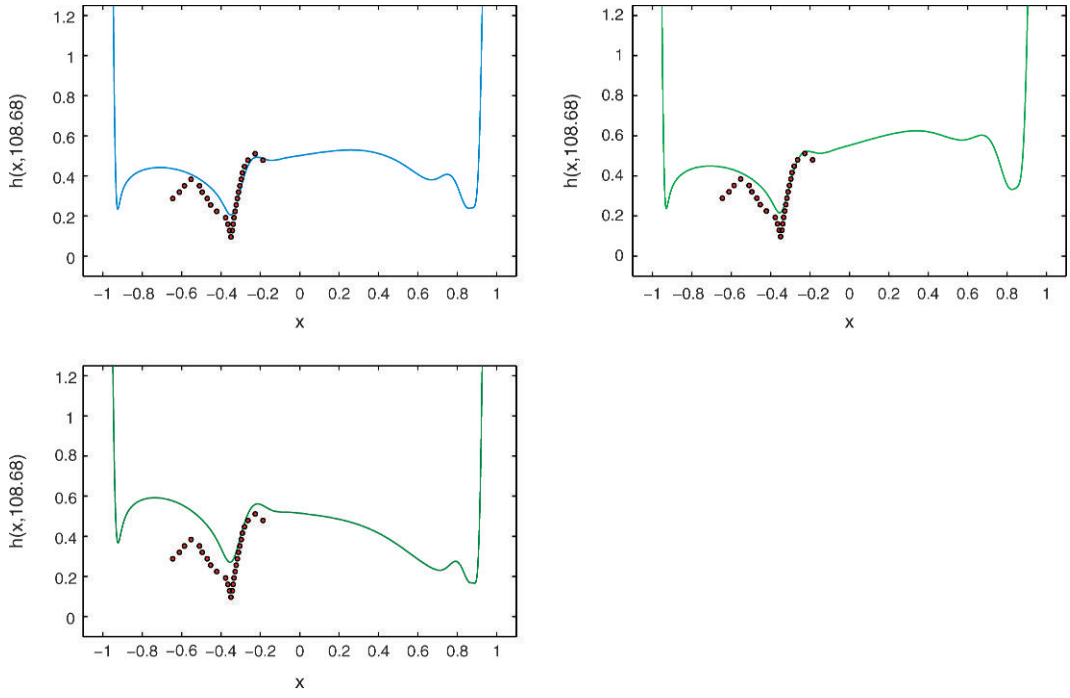

FIG. 11. Results for partial blinks beginning with $\lambda_0 = 0.1$ and then repeating at $\lambda = 0.5$ thereafter for FPLM boundary conditions. Top left: $h_e = 0.25$, $V_0 = 1.576$. Top right: $h_e = 0.25$, $V_0 = 1.776$. Bottom left: $h_e = 0.35$, $V_0 = 1.576$.

align with the minimum in each case, and the curve shows computed results at $t = 108.68$, just when the lids fully open for the second time; in another 20 time units (or 1 s), the black lines form at the ends, but the valley region is essentially unchanged. This corresponds roughly to the time of measurement after a filmed half blink (Braun & King-Smith, 2007). In the top-left panel, $V_0 = 1.576$ and $h_e = 0.25$, corresponding to a 2.5-μm film away from the menisci when the lids are fully open and a 1.25-μm film under the edge of the lid. The top panels show that the minima are not deep enough compared to the experimental data but the slope on the right side is roughly correct. Varying the tear volume changes the thickness at either side of the valley and the overall thickness to the right of the valley. Increasing h_e as in the bottom-left panel leaves the valley shape with a poorer comparison with the observed thickness. We note that the film thickness at the ends may be quite small once the black line has formed in all these cases, e.g. under 0.1 (i.e. 0.5 μm dimensionally).

Figure 12 shows a comparison with the half blink experiment for FPLM+ boundary conditions that were modified for the partial blink case. We used $\beta = 10^{-3}$, $Q_{0\mathrm{lg}} = 0.337$, $Q_{0\mathrm{p}} = 0.0297$, $f_{\mathrm{top}} = 0.6$ and $f_{\mathrm{out}} = 0.65$ for the initial upstroke from the fully closed position ($\lambda_0 = 0.1$) and the open phase. For the subsequent half blinks, the punctal flux was set to zero and the lacrimal gland influx was reduced to 25% of its value (i.e. $Q_{0\mathrm{lg}} \to Q_{0\mathrm{lg}}/4$ and $Q_{0\mathrm{p}} \to 0$ for half blinks). We chose these fluxes because the puncta are assumed to not empty and refill during a half blink and the lacrimal gland is assumed to supply a smaller amount of tear fluid for a half blink. The results show that the agreement in the vicinity of the minimum film thickness is improved, both in the minimum value and in the overall shape of the valley. The film thickness at each side of the valley is larger than the experiment, the minimum

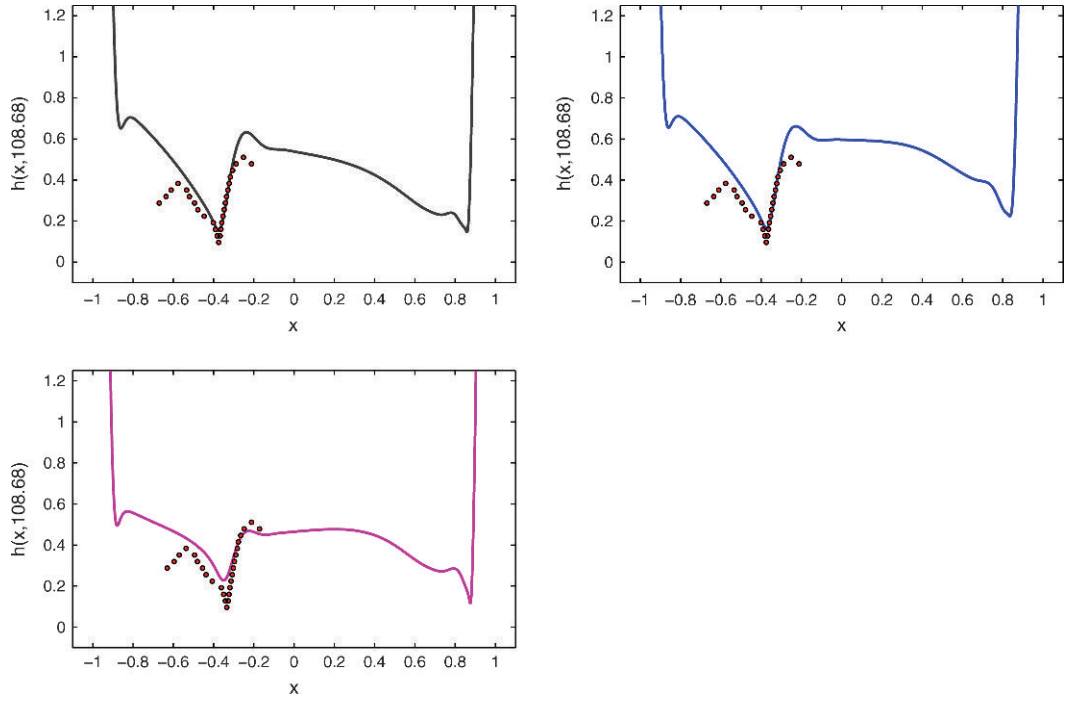

FIG. 12. Film thickness as a function of x while the moving end is fully open with FPLM+ boundary conditions. Top left: $h_e = 0.35$, $V_0 = 1.576$. Top right: $h_e = 0.35$, $V_0 = 1.776$. Bottom left: $h_e = 0.2$, $V_0 = 1.376$.

valley thickness is a little larger and the film thickness near the stationary end is under 0.5 μm thick dimensionally, however.

If we relax the expectation that the best comparison with experiment should occur after the first half blink, better comparisons with the *in vivo* thicknesses can be made. As an example, consider the results in Fig. 13; here, $S = 2 \times 10^{-5}$, $\beta = 10^{-3}$, $h_e = 0.4$, $V_0 = 1.576$, $f_{\text{top}} = 0.7$, $f_{\text{out}} = 0.75$ and all other parameters as for FPLM+ boundary conditions as described above. The shape and size of the valley improve with successive half blinks. This improvement does not occur for FPLM boundary conditions.

It may be noted that there has been some variability in the thickness distributions in the half blinks that we have observed. In some cases, the distribution approximates a ramp which is thickest at the top, with a sharp transition to a more uniform tear film below the ramp, and further analysis of these distributions is planned in future work.

4.1.3 *Full blink equivalence.* Braun (2006) first found that periodic solutions occurred when the fully closed state had a sufficiently small opening remaining; the dependence on the volume of the tear film was studied by Braun & King-Smith (2007). In both these papers, sinusoidal lid motion was used. The periodic solutions were interpreted to be fluid dynamically equivalent to a full blink.

In this section, we study the effect of realistic lid motion on how large the minimum opening of the tear film should be for periodic solutions in the USL. Our approach is more quantitative in this work; we compute the ℓ_∞-norm of the difference between two solutions that are separated by the duration of a blink cycle, denoted Δ. When the difference is small, the solutions are essentially periodic. The quantity

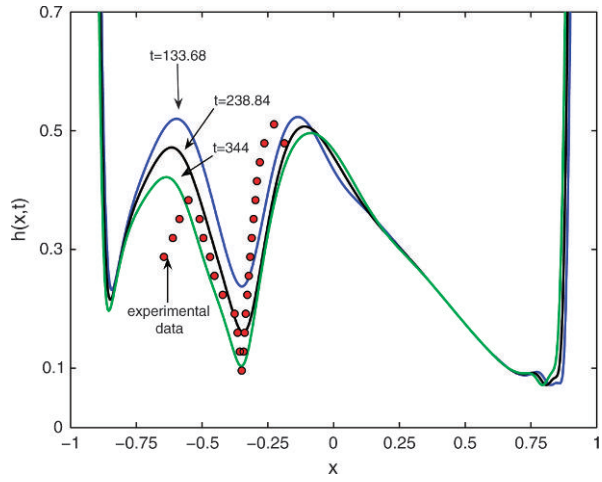

FIG. 13. Results at fully open domains for multiple half blinks. Initially, the eye was fully closed, then opened, then repeated half blinks began. The shape of the valley improves with successive half blinks.

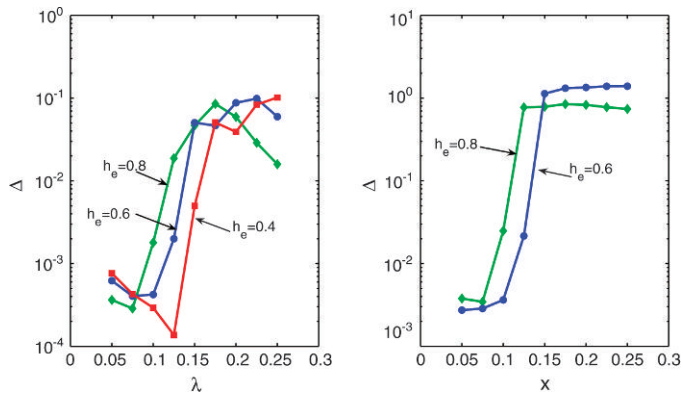

FIG. 14. The norm of the difference between two film thickness profiles separated by a blink cycle as a function of λ for $S = 10^{-5}$. Left: For FPLM boundary conditions, a plunge occurs in the norm of the difference at around $\lambda = 0.15$ for $h_e = 0.4$ and around $\lambda = 0.125$ for $h_e = 0.8$; this result is similar to the results of Braun & King-Smith (2007). Right: A similar plunge occurs for FPLM+ boundary conditions. For the latter, we used $Q_{0\mathrm{lg}} = 0.337$, $Q_{0\mathrm{p}} = 0.0297$, $f_{\mathrm{top}} = 0.6$ and $f_{\mathrm{out}} = 0.5$ in all data points for this plot.

Δ is given by

$$\Delta = ||H(\xi, 2\Delta t_{\mathrm{bc}} + \Delta t_{\mathrm{co}}) - H(\xi, \Delta t_{\mathrm{bc}} + \Delta t_{\mathrm{co}})||_{\infty}. \tag{4.32}$$

In Fig. 14, the norm of difference between solutions is shown as a function of λ; each curve is for a different value of h_e with the timescale and blink cycle duration used in this paper.

On the left is the result for FPLM boundary conditions. We see that there is a rapid decrease in the difference of about two orders of magnitude in the interval $0.125 \leqslant \lambda \leqslant 0.175$. We conclude that at about 1/6 to 1/8 of the eye surface remaining open, the solutions become essentially periodic. This is

a larger value than was found for sinusoidal lid motion (Braun, 2006; Braun & King-Smith, 2007). On the right in Fig. 14, the results for the FPLM+ boundary conditions are similar, with perhaps a slightly smaller value of λ where periodicity begins.

4.2 *Stress-free limit*

Film profiles are shown in Fig. 15 for the SFL with $\lambda = 0.1$ and with FPLM boundary conditions for $h_e = 0.8$. The film is laid down during the upstroke (top panel), and the film tends to be thicker towards the bottom of the film (the stationary end). In the USL case, these parameters and boundary conditions yielded an essentially flat film away from the menisci upon opening. The capillary-driven relaxation and thinning at the ends occur in the middle panel, and this process is faster than that in the USL case. Finally, the blink cycle is completed in the bottom panel; this panel in particular is new to this work. The film is 'rolled up' into or 'laid down' out of the meniscus but it is not stretched, as previously described for the simplified lid motion of Braun (2006) and Braun & King-Smith (2007).

The time sequence of results for a partial blink with FPLM boundary conditions and $h_e = 0.6$ is shown in Fig. 16. A number of points may be made from this figure. The middle panel illustrates a difficulty with FPLM boundary conditions during the downstroke of the moving end. An oscillatory deformation occurs where the meniscus joins the rest of the film in all cases; for FPLM boundary conditions, this oscillation may be pronounced, and it becomes more pronounced with increasing h_e, decreasing S and decreasing V_0. The likelihood of film rupture is increased when this occurs, and this feature limits the utility of FPLM boundary conditions for the full blink cycle in some cases.

The bottom panel of Fig. 16 shows how the valley in the middle of the film develops from a half blink for the SFL. The sloping left side of the valley is left behind as the moving end retreats from the centre of the film. This gradual thickness increase is not very similar to the observed tear film profiles, as discussed in what follows. We also note that the relative minimum in the tear film thickness from the half blink remains essentially in the middle of the film, while in the USL, that relative minimum is shifted towards the moving end. It may be possible to observe this shift, or lack of it, with sufficiently high speed and sensitive cameras observing the tear film *in vivo*; we are unable to resolve this issue with the equipment currently available to us.

We now turn to the comparison of computed half blink results with measurements made *in vivo* for the SFL with two different flux boundary conditions. In the upper part of Fig. 17, FPLM boundary conditions are used with $h_e = 0.6$; the resulting film profile has a valley in the middle of the film, but the thickness at the middle is too thin, and the left side of the valley is not shaped like the measured PLTF thickness. The lower part of the figure shows results for the FPLM+ boundary conditions that are the same as those in Fig. 12 for the USL. These boundary conditions include a quarter of the full blink influx and no punctal drainage during the half blink parts of the blink cycles (as before). The resulting film profile near the relative minimum is better than that for FPLM boundary conditions alone, with the minimum being closer to the measured value and the shape of the left side being steeper and a little closer to the measured profile. In the latter SFL result, the right side of the valley has roughly the right slope.

4.3 *Comparison with Wong, Fatt and Radke*

At this point, we may compare the results of the previous models with the coating flow model of film formation from Wong *et al.* (1996). Writing their equation (8) in terms of our variables gives

$$h = 2.1234 \frac{\epsilon^2 R'}{d'} \left(\frac{X_t}{S} \right)^{2/3}. \tag{4.33}$$

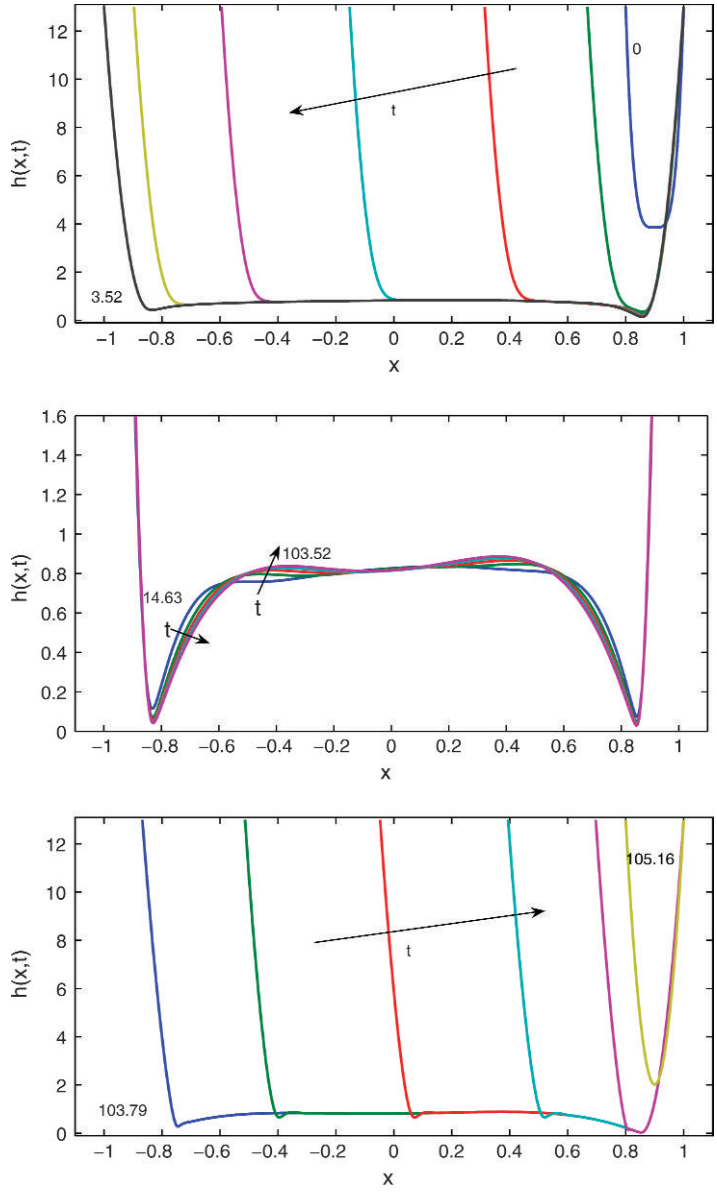

FIG. 15. SFL results for a full blink cycle using FPLM boundary conditions with $h_e = 0.8$ and $V_0 = 2.576$ in analogy with Fig. 5. Top: Upstroke of the blink cycle. Middle: Zoom in the vertical direction for various times while the domain is fully open. Bottom: The downstroke of the blink cycle.

We note that this is for a tangentially immobile surface, corresponding most closely to the USL limit, but we make comparisons for both limits from this work. We use $R' = 0.25$ mm, $\epsilon = 10^{-3}$, $d' = 5$ μm, X_t is the speed of the upper lid for $\lambda = 0.1$, and we vary S from 2×10^{-5} (slower lid motion) to 5×10^{-7} (faster lid motion). The comparison with our computations for full blinks with FPLM boundary

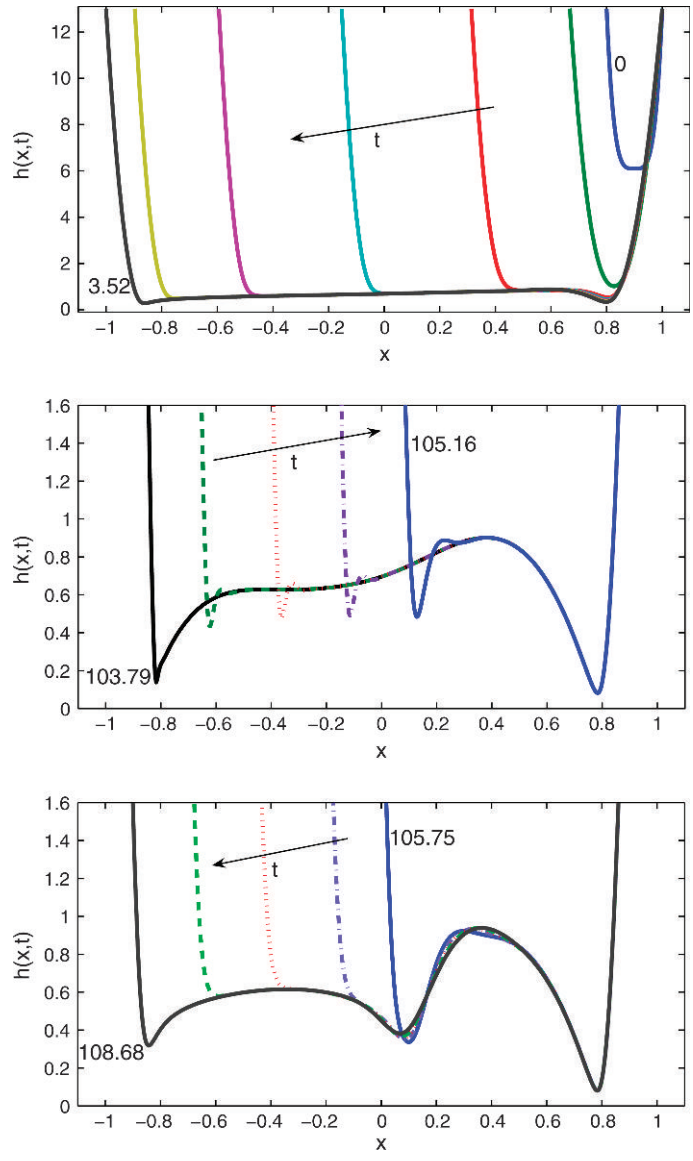

FIG. 16. SFL results for a half blink following a full blink. We begin from the closed position with $\lambda_0 = 0.1$ and after the initial opening, $\lambda = 0.5$. Top: Upstroke from fully closed position. Middle: Downstroke to the halfway point ($\lambda = 0.5$) after the initial upstroke and open phase (the latter two were shown in the upper two panels of the previous figure). Bottom: Upstroke after half closing.

conditions is shown in Fig. 18. We note that our function $X_t(x)$ (adapted for incomplete closure from Berke & Mueller, 1998) is more symmetric than that measured by Wong *et al.*, and this is reflected in the values we compute from their formula. We find that at smaller S values, our computed results are thinner, while those at larger S are thicker. We believe that this is a consequence of dynamic interaction of the film with the meniscus, which is not included in the deposition model of Wong *et al.* (1996).

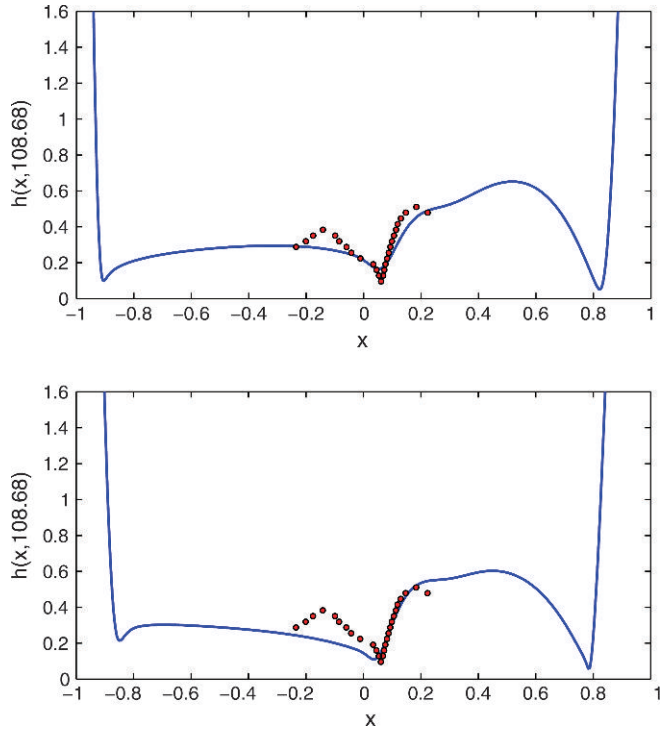

FIG. 17. SFL results for partial blinks beginning with $\lambda_0 = 0.1$ and then repeating at $\lambda = 0.5$ thereafter for FPLM boundary conditions. $S = 2 \times 10^{-5}$ and $h_e = 0.25$ in both cases. Top: $V_0 = 1.776$ using FPLM boundary conditions. Bottom: $V_0 = 1.776$ using FPLM+ boundary conditions with $Q_{0\mathrm{lg}} = 0.337$, $Q_{0\mathrm{p}} = 0.0297$, $f_{\mathrm{top}} = 0.6$ and $f_{\mathrm{out}} = 0.65$ on the initial upstroke and open phase and then an influx with magnitude $0.25Q_{0\mathrm{lg}}$ and no outflux ($Q_{0\mathrm{p}} = 0$) for each subsequent partial blink. This latter case is analogous to Fig. 12.

5. Discussion

Some of our results agree with the computed solutions of tear film formation and relaxation found by Jones *et al.* (2005). For example, slow capillary thinning after the upstroke near the ends of the film is reminiscent of black line formation in eyes, as has been discussed by a number of authors (Wong *et al.*, 1996; Sharma *et al.*, 1998; Braun & Fitt, 2003; Miller *et al.*, 2003; Jones *et al.*, 2005). The findings in this work support the concept of FPLM boundary conditions that Jones *et al.* introduced. The flux of tear fluid from under the lid seems to be a major component of creating a reasonably uniform tear film. We added additional fluxes that are smaller than the FPLM contribution from beneath the upper lid, but they do increase the realism of the fluxes for both ends of the film to include supply from the lacrimal gland and the drainage into the puncta. We also note that our assumption of a constant value of h_e throughout the blink cycle, following Jones *et al.* (2005, 2006), is likely to be a simplification of lid position relative to the cornea in a real blink where that spacing may be time dependent.

We tuned the fluxes into and out of the ends to what seemed to be sensible values. We typically assigned 60–75% of the influx of new tear fluid from the lacrimal glands into the top end of the film, while the outflux was 50–65% from the top. The latter did help prevent rupture of the film in some cases at the stationary end (x or $\xi = 1$). However, in eyes, more tear fluid is drained from the lower puncta, and so it may be more realistic to have $f_{\mathrm{out}} < 0.5$ (Zhu & Chauhan, 2005; Nagashima & Kido, 1984).

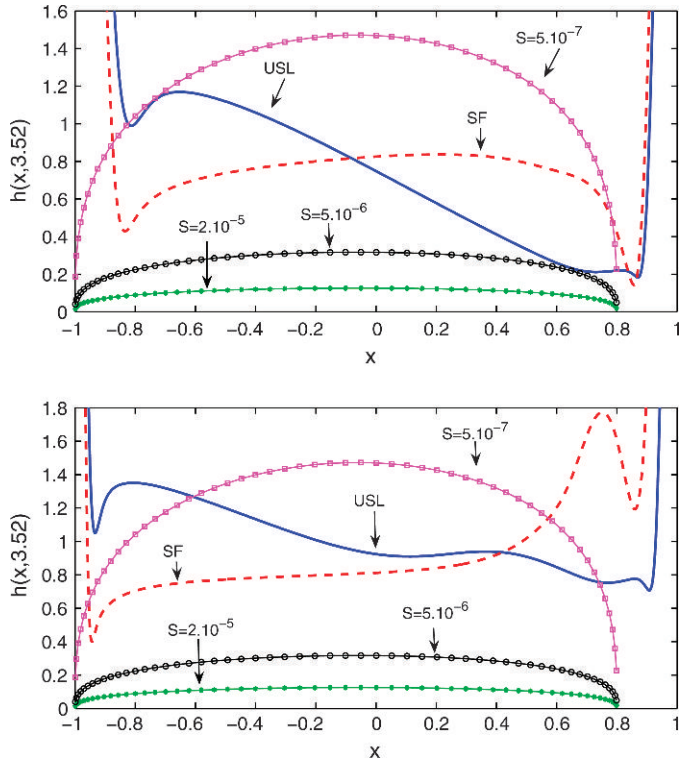

FIG. 18. Comparison of our computed results with the results of Wong *et al.* (1996); results from their formula (8) are shown as solid curves with symbols for different S. Top: $S = 2 \times 10^{-5}$ for both USL and SF results at $t = 3.52$ corresponding to the parameters of Figs 5 and 12, respectively. Bottom: $S = 5 \times 10^{-7}$ for both USL and SF results at $t = 3.52$.

Detailed partitioning of the supply and drainage of new and excess tear fluid will only be determined by 2D film models, not by the 1D films employed here.

When the eye does not 'fully close' enough to cause periodic behaviour, we consider the blink to be 'partial'. In the partial blink case, the film behaviour has a swept part that is approximately periodic and an unswept part that is driven by the capillary forces which dominate in drainage flow after a blink (Braun & Fitt, 2003; Wong *et al.*, 1996; Sharma *et al.*, 1998; Miller *et al.*, 2003; McDonald & Brubaker, 1971). This behaviour was found with both sinusoidal lid motion and fluxes (Braun, 2006; Braun & King-Smith, 2007) and in the current case with more realistic lid motion and fluxes. With realistic lid motion and fluxes, $\lambda \approx 1/6$ to $1/8$ was the boundary between periodic and non-periodic solutions; for the sinusoidal motion in our previous work, we found this transition to occur for values as low as $\lambda \approx 1/8$. From a fluid dynamic perspective, this is the minimum amount of closure required to completely renew the tear film after each blink cycle; this may be a partial explanation as to why many blinks do not have the lids completely closed (Doane, 1980).

In the absence of any flux through the stationary end of the film, there is a slow decay of the minimum film thickness driven only by capillarity. When a non-zero flux leaving the film is added to the stationary end, the decrease in h is accelerated and a series of partial blinks in this case leads to rupture of the film near that end. Thus, these models, depending on the conditions, may have rupture occurring near either end of the film; Jones *et al.* (2005) arrived at this conclusion also from studying tear film formation and

relaxation only. While tear film break-up (rupture) in eyes may often occur away from film ends (Bitton & Lovasik, 1998), there is experimental evidence for break-up near the ends (see e.g. McDonald & Brubaker, 1971; King-Smith *et al.*, 2005).

Distinctive features have been observed in the tear film when the upper lid only performs a half blink. A valley is left behind in the surface of the tear film, which has been computed for sinusoidal lid motions and fluxes (Braun, 2006; Braun & King-Smith, 2007) along with realistic lid motion and a mobile surface with a surfactant (Jones *et al.*, 2006). The models in this paper improved upon our prior comparisons with quantitative *in vivo* thickness measurements for a PLTF after a half blink (Braun & King-Smith, 2007). The computations by Jones *et al.* (2006) used a 10-μm film, and their fluorescence-based method could only provide qualitative information; within those limitations, the comparison was good. In this work, we made detailed comparison with quantitative *in vivo* measurements of a PLTF. In general terms, the comparison between the computations and the measurements improves if there is a tear film around 3 μm thick on the average and there is a small influx of tear fluid from the lacrimal gland during the half blink. The USL had better agreement with the shape of the valley than the SFL did. We concur with the findings of Jones *et al.* (2005) that the overall film thickness profiles from the USL are a better match to observed tear film thickness behaviour than those from the SFL. Further refinements in the modelling, such as shear thinning tear fluid or a separate lipid layer with a surfactant, and more detailed experimental observations may improve the agreement beyond the immediate vicinity of the valley left behind by the half blink.

6. Conclusion

In this paper, we developed a new numerical method for the problem of computing solutions for the tear film over multiple blink cycles with realistic lid motions. We generalized the flux boundary conditions posed by Jones *et al.* (2005) to include an average supply from the lacrimal gland and the drainage due to the puncta. We found that there were differences in the evolution near the end of the upstroke, but the differences were minimized by the end of the open phase of the blink cycle.

The tear film had periodic solutions if sufficient closure occurred during the blink cycle, with periodicity being lost if the ends were not sufficiently close as in our previous work with sinusoidal models for the lid motion (Braun, 2006; Braun & King-Smith, 2007). The fraction of closure required for periodicity does not seem to be very sensitive to the kind of lid motion used; the transitions for sinusoidal motion are similar to the values found for the USL case investigated here. Knowledge of these transitions may suggest useful values in clinical settings for what range of blinks works as effectively as completely closed lids for the purpose of regenerating the tear film.

Our effort to improve the comparison with quantitative measurements of the tear film thickness after a half blink seemed to require, at least in our model, the new features we have added. The quantitative comparison of some aspects in the vicinity of the valley was good, but the comparison with the overall film profile could still be improved.

Extensions using a mobile surface with surfactant transport will continue to yield new insights, as will extension to a 2D film on an eye-shaped domain. We are currently working in these directions, particularly to implement computational models of the tear film that include the tear film supply and drainage cycle described by Doane (1981).

Acknowledgements

RJB thanks M. G. Doane for helpful conversations. PEKS thanks J. J. Nichols, K. K. Nichols, B. A. Fink and R. M. Hill for their advice and assistance.

Funding

National Science Foundation (DMS-0616483).

REFERENCES

BAYLISS, A., CLASS, A. & MATKOWSKY, B. J. (1995) Roundoff error in computing derivatives using the Chebyshev differentiation matrix. *J. Comput. Phys.*, **116**, 380–383.

BENEDETTO, D. A., CLINCH, T. E. & LAIBSON, P. R. (1984) In vivo observation of tear dynamics using fluorophotometry. *Arch. Ophthalmol.*, **102**, 410–412.

BERGER, R. E. & CORRSIN, S. (1974) A surface tension gradient mechanism for driving the pre-corneal tear film after a blink. *J. Biomech.*, **7**, 225–238.

BERKE, A. & MUELLER, S. (1996) Einfluss des lidschlages auf die kontaktlinse und die zugrundeliegenden kräfte. *Kontaktlinse*, **1**, 17–26.

BERKE, A. & MUELLER, S. (1998) The kinetics of lid motion and its effects on the tear film. *Lacrimal Gland, Tear Film, and Dry Eye Syndromes 2* (D. A. Sullivan, D. A. Dartt & M. A. Meneray eds). New York: Plenum Press, pp. 417–424.

BITTON, E. & LOVASIK, J. V. (1998) Longitudinal analysis of precorneal tear film rupture patterns. *Lacrimal Gland, Tear Film and Dry Eye Syndromes 2* (D. A. Sullivan, D. A. Dartt & M. A. Meneray eds). New York: Plenum Press, pp. 381–389.

BRAUN, R. J. (2006) Models for human tear film dynamics. *Wave Dynamics and Thin Film Flow Systems* (R. Usha, A. Sharma & B. S. Dandapat eds). Chennai, India: Narosa, pp. 404–434.

BRAUN, R. J. & FITT, A. D. (2003) Modelling drainage of the precorneal tear film after a blink. *Math. Med. Biol.*, **20**, 1–28.

BRAUN, R. J. & KING-SMITH, P. E. (2007) Model problems for the tear film in a blink cycle: single equation models. *J. Fluid Mech.*, **586**, 465–490.

BRON, A. J., TIFFANY, J. M., GOUVEIA, S. M., YOKOI, N. & VOON, L. W. (2004) Functional aspects of the tear film lipid layer. *Exp. Eye Res.*, **78**, 347–360.

CHEN, H. B., YAMABAYASHI, S., OU, B., TANAKA, Y. & OHNO, S. (1997) *In vivo* tear-film thickness determination and implications for tear-film stability. *Invest. Ophthalmol. Vis. Sci.*, **38**, 381–387.

CREECH, J. L., DO, L. T., FATT, I. & RADKE, C. J. (1998) *In vivo* tear-film thickness determination and implications for tear-film stability. *Curr. Eye Res.*, **17**, 1058–1066.

DOANE, M. G. (1980) Interaction of eyelids and tears in corneal wetting and the dynamics of the normal human eyeblink. *Am. J. Ophthalmol.*, **89**, 507–516.

DOANE, M. G. (1981) Blinking and the mechanics of the lacrimal drainage system. *Ophthalmology*, **88**, 844–851.

DON, W. S. & SOLOMONOFF, A. (1995) Accuracy and speed in computing the Chebyshev collocation derivative. *SIAM J. Sci. Comput.*, **16**, 1253–1268.

DON, W. S. & SOLOMONOFF, A. (1997) Accuracy enhancement for higher derivatives using Chebyshev collocation and a mapping technique. *SIAM J. Sci. Comput.*, **18**, 1040–1055.

EHLERS, N. (1965) The precorneal film: biomicroscopical, histological and chemical investigations. *Acta Ophthalmol. Suppl.*, **81**, 3–135.

FATT, I. & WEISSMAN, B. A. (1992) *Physiology of the Eye—An Introduction to the Vegetative Functions*, 2nd edn. Boston, MA: Butterworth-Heinemann.

GIPSON, I. K. (2004) Distribution of mucins at the ocular surface. *Exp. Eye Res.*, **78**, 379–388.

HERYUDONO, A. (2008) *Ph.D. Thesis*, Department of Mathematical Sciences, University of Delaware.

HOLLY, F. J. (1973) Formation and rupture of the tear film. *Exp. Eye Res.*, **15**, 515–525.

HOLLY, F. J. & LEMP, M. A. (1977) Tear physiology and dry eyes. *Surv. Ophthalmol.*, **22**, 69–87.

HUH, C. & SCRIVEN, L. E. (1971) Hydrodynamic model of a steady movement of a solid/liquid/fluid contact line. *J. Colloid. Interface Sci.*, **35**, 85–101.

JONES, M. B., MCELWAIN, D. L. S., FULFORD, G. R., COLLINS, M. J. & ROBERTS, A. P. (2006) The effect of the lipid layer on tear film behavior. *Bull. Math. Biol.*, **68**, 1355–1381.

JONES, M. B., PLEASE, C. P., MCELWAIN, D. L. S., FULFORD, G. R., ROBERTS, A. P. & COLLINS, M. J. (2005) Dynamics of tear film deposition and draining. *Math. Med. Biol.*, **22**, 265–288.

KESSING, S. V. (1967) A new division of the conjuctiva on the basis of x-ray examination. *Acta Ophthalmol. (Copenh.)*, **45**, 680–683.

KING-SMITH, P. E., FINK, B. A. & FOGT, N. (1999) Three interferometric methods for measuring the thickness of layers of the tear film. *Optom. Vis. Sci.*, **76**, 19–32.

KING-SMITH, P. E., FINK, B. A., HILL, R. M., KOELLING, K. W. & TIFFANY, J. M. (2004) The thickness of the tear film. *Curr. Eye Res.*, **29**, 357–368.

KING-SMITH, P. E., FINK, B. A., HILL, R. M., KOELLING, K. W. & TIFFANY, J. M. (2005) Reply to letter by Dr. C. J. Radke. *Curr. Eye Res.*, **30**, 1133–1134.

KING-SMITH, P. E., FINK, B. A., NICHOLS, J. J., NICHOLS, K. K. & HILL, R. M. (2006) Interferometric imaging of the full thickness of the precorneal tear film. *J. Opt. Soc. Am. A*, **23**, 2097–2104.

KOSLOFF, D. & TAL-EZER, H. (1993) A modified Chebyshev pseudospectral method with an $O(N^{-1})$ time step restriction. *J. Comput. Phys.*, **104**, 457–469.

LEVICH, V. G. (1962) *Physicochemical Hydrodynamics*. Englewood Cliffs, NJ: Prentice Hall.

LORBER, M. (2007) Gross characteristics of normal human lacrimal glands. *Ocul. Surf.*, **5**, 13–22.

MAURICE, D. M. (1973) The dynamics and drainage of tears. *Int. Ophthalmol. Clin.*, **13**, 103–116.

MCCULLEY, J. P. & SHINE, W. (1997) A compositional based model for the tear film lipid layer. *Trans. Am. Ophthalmol. Soc.*, **XCV**, 79–93.

MCDONALD, J. E. & BRUBAKER, S. (1971) Meniscus-induced thinning of tear films. *Am. J. Ophthalmol.*, **72**, 139–146.

MILLER, K. L., POLSE, K. A. & RADKE, C. J. (2003) On the formation of the black line. *Curr. Eye Res.*, **25**, 155–162.

MISHIMA, S. (1965) Some physiological aspects of the precorneal tear film. *Arch. Ophthalmol.*, **73**, 233–241.

MISHIMA, S., GASSET, JR., A., KLYCE, S. D. & BAUM, J. L. (1966) Determination of tear volume and tear flow. *Invest. Ophthalmol.*, **5**, 264–276.

MÜNCH, A., WAGNER, B. & WITELSKI, T. P. (2005) Lubrication models with small to large slip lengths. *J. Eng. Math.*, **53**, 359–383.

NAGASHIMA, K. & KIDO, R. (1984) Relative roles of the upper and lower canaliculi in normal tear drainage. *Jpn. J. Ophthalmol.*, **28**, 259–262.

NORN, M. S. (1966) The conjuctival fluid, its height, volume, density of cells, and flow. *Acta Ophthalmol. (Copenh.)*, **44**, 212–222.

OWENS, H. & PHILLIPS, J. (2001) Spread of the tears after a blink: velocity and stabilization time in healthy eyes. *Cornea*, **20**, 484–487.

PROBSTEIN, R. F. (1994) *Physicochemical Hydrodynamics*. New York: Wiley.

ROLANDO, M. & REFOJO, M. F. (1983) Tear evaporimeter for measuring water evaporation rate from the tear film under controlled conditions in humans. *Exp. Eye Res.*, **36**, 25–33.

SHARMA, A., KHANNA, R. & REITER, G. (1999) A thin film analog of the corneal mucus layer of the tear film: an enigmatic long range non-classical dlvo interaction in the breakup of thin polymer films. *Colloids Surf. B Interfaces*, **14**, 223–235.

SHARMA, A., TIWARI, S., KHANNA, R. & TIFFANY, J. M. (1998) Hydrodynamics of meniscus-induced thinning of the tear film. *Lacrimal Gland, Tear Film, and Dry Eye Syndromes 2* (D. A. Sullivan, D. A. Dartt & M. A. Meneray eds). New York: Plenum Press, pp. 425–431.

WONG, H., FATT, I. & RADKE, C. J. (1996) Deposition and thinning of the human tear film. *J. Colloid Interface Sci.*, **184**, 44–51.

ZHANG, L., MATAR, O. K. & CRASTER, R. (2003) Surfactant driven flows overlying a hydrophobic epithelium: film rupture in the presence of slip. *J. Colloid Interface Sci.*, **264**, 160–175.

ZHU, H. & CHAUHAN, A. (2005) A mathematical model for tear drainage through the canaliculi. *Curr. Eye Res.*, **30**, 621–630.

Appendix A. Derivation of USL model

When the Marangoni effect is very strong, there is another simplification to a single equation. This USL was first proposed by Jones *et al.* (2005) to our knowledge, but they did not give a derivation of this limit and we give one here. The tangential stress condition, $u_y = M\Gamma_x$, requires $\Gamma_x = 0$ on the free surface in this limit to leading order. The surfactant transport equation becomes

$$\Gamma_t + u_x^{(s)}\Gamma = 0. \tag{A.1}$$

Because the concentration is spatially uniform to leading order 'but still time varying', we may write

$$\Gamma = \frac{2}{1 - X(t)}\Gamma_m \quad \text{and} \quad \frac{\mathrm{d}\Gamma}{\mathrm{d}t} = \frac{2}{(1 - X(t))^2}X_t\Gamma_m. \tag{A.2}$$

Here, Γ_m is a constant and is the minimum concentration during the cycle (fully extended domain). Substitution into the surfactant transport equation gives

$$u_x^{(s)} = -\frac{X_t}{1 - X}; \tag{A.3}$$

solving the ODE for $u^{(s)}$ and using $u^{(s)}(1, t) = 0$ give

$$u^{(s)} = X_t\frac{1 - x}{1 - X}. \tag{A.4}$$

Computing the flux yields $q^{(2)}(x, t)$ as given in (2.10); substituting into (2.8) yields the single PDE for $h(x, t)$ for the USL case. Note that if $X_t = 0$, we recover the equation for the free surface with slip on the bottom surface but a tangentially immobile ($M \gg 1$) free surface. If $\beta = 0$ as well, we recover the tangentially immobile case with a no-slip bottom surface.

Appendix B. Mapped spectral method

We now describe the spectral collocation method that we employed to solve the equations in DAE form, as in (3.25) and (3.26). Kosloff & Tal-Ezer (1993) pointed out that if solutions have high gradients away from boundaries or solutions are smooth throughout the interval, there is no need to cluster collocation points near boundaries as with Chebyshev points. They proposed a simple method to transform Chebyshev points to another set of points in $[-1, 1]$ such that its minimal spacing near boundaries is larger, specifically $\mathrm{O}(N^{-1})$. Their simplest method uses a symmetric transformation

$$\psi = g(\xi; \alpha) = \frac{\sin^{-1}(\alpha\xi)}{\sin^{-1}(\alpha)}, \quad \psi, \xi \in [-1, 1]. \tag{B.1}$$

By using the chain rule, we obtain

$$\frac{\mathrm{d}f}{\mathrm{d}\psi} = \frac{1}{g'(\xi;\alpha)}\frac{\mathrm{d}f}{\mathrm{d}\xi} \tag{B.2}$$

for any given $f \in C^1[-1,1]$. Hence, at node points ψ_i our discrete kth derivative vectors become

$$H^{(k)} = A^k D^{(k)} H \quad \text{and} \quad Q^{(k)} = A^k D^{(k)} Q, \tag{B.3}$$

where $D^{(k)}$ is the kth derivative matrix using standard Chebyshev collocation without mapping and A is a diagonal matrix with diagonal elements

$$A_{ii} = \frac{1}{g'(\xi_i;\alpha)}. \tag{B.4}$$

By suitable choice of α, the minimal spacing of ψ_i can be stretched to

$$\Delta\psi_{\min} = \mathrm{O}(N^{-1}), \tag{B.5}$$

which also serves as a new time-marching stability condition. In our experience, the technique also improves the performance of time-implicit schemes.

Computing kth derivatives using Chebyshev spectral collocation methods suffers from roundoff error of $\mathrm{O}(N^{2k})$ (Bayliss *et al.*, 1995; Don & Solomonoff, 1995). Roundoff contamination can ruin practical computations in double precision even for $k = 3$ or 4; this played a large role in our preference for the DAE form rather than imposing boundary conditions on h_{xxx}. The modified collocation method using the mapping of Kosloff & Tal-Ezer (1993) does not suffer from this theoretical minimum. Don & Solomonoff (1997) showed that if one chooses

$$\alpha = \mathrm{sech}\left(\frac{-\log\epsilon_{\mathrm{m}}}{N}\right), \tag{B.6}$$

where ϵ_{m} is the machine precision, then the roundoff errors in computing kth derivatives become $\mathrm{O}((-N\log\epsilon_{\mathrm{m}})^k)$.

There is a significant asymmetry in our problem introduced by the moving end of the domain. Kosloff & Tal-Ezer (1993) also proposed a non-symmetric mapping of the form

$$\psi = g(\xi;\alpha,\beta) = \frac{1}{a}\left(\sin^{-1}\left(\frac{2\alpha\beta\xi + \alpha - \beta}{\alpha+\beta}\right) - b\right), \quad \psi,\xi \in [-1,1], \tag{B.7}$$

$$a = \frac{1}{2}\left(\sin^{-1}\left(\frac{2\alpha\beta + \alpha - \beta}{\alpha+\beta}\right) - \sin^{-1}\left(\frac{-2\alpha\beta + \alpha - \beta}{\alpha+\beta}\right)\right), \tag{B.8}$$

$$b = \frac{1}{2}\left(\sin^{-1}\left(\frac{2\alpha\beta + \alpha - \beta}{\alpha+\beta}\right) + \sin^{-1}\left(\frac{-2\alpha\beta + \alpha - \beta}{\alpha+\beta}\right)\right), \tag{B.9}$$

where α and β control distribution points near $\xi = 1$ and $\xi = -1$, respectively. If $\alpha = \beta$, we recover the standard symmetric mapping (B.1). The lid motion tends to produce steeper gradients near $\xi = -1$ than near $\xi = 1$, and while we could sometimes use $\alpha = \beta$, we found that our typical choice of $\alpha = 0.3$ and $\beta = 0.1$ gave better performance in some numerical experiments.

We also used homogenization of the boundary conditions to improve the accuracy of the derivatives at and near the end points of the domain. Homogenization can be done by shifting variables H and Q such that

$$\hat{H} = H - h_0, \tag{B.10}$$

$$\hat{Q} = Q - (a\xi + b). \tag{B.11}$$

It is clear that $\hat{H}(\pm 1, t) = 0$. In order to find a and b such that $\hat{Q}(\pm 1, t) = 0$, we end up solving 2×2 system of linear equations consisting of $a + b = Q^{(i)}(1, t)$ and $-a + b = Q^{(i)}(-1, t)$. Hence, (3.25) and its initial condition (3.28) in $-1 < \xi < 1$ become

$$\hat{H}_t = \frac{1-\xi}{1-X} X_t \hat{H}_\xi - \left(\frac{2}{1-X}\right) \hat{Q}^{(i)}_\xi - \left(\frac{1}{1-X}\right) (Q^{(i)}(1, t) - Q^{(i)}(-1, t)), \tag{B.12}$$

$$\hat{H}(\xi, 0) = H(\xi, 0) - h_0 \tag{B.13}$$

with homogeneous boundary conditions $\hat{H}(\pm 1, t) = \hat{Q}(\pm 1, t) = 0$.